Contents lists available at ScienceDirect

# Journal of Controlled Release

journal homepage: www.elsevier.com/locate/jconrel





# Cell-specific mRNA delivery via nanobody-functionalized lipid nanoparticles

Linglong Chen <sup>a,\*</sup>, Hans Van Der Weken <sup>a</sup>, Olivier Zwaenepoel <sup>b</sup>, Irina A. Okkelman <sup>d</sup>, Justine Aelvoet <sup>c</sup>, Emma Van Denberghe <sup>a</sup>, Jan Gettemans <sup>b</sup>, Ruslan I. Dmitriev <sup>d</sup>, Bruno G. De Geest <sup>c</sup>, Eric Cox <sup>a</sup>, Bert Devriendt <sup>a</sup>

- <sup>a</sup> Laboratory of Immunology, Faculty of Veterinary Medicine, Ghent University, Salisburylaan 133, 9820 Merelbeke, Belgium.
- b Department of Biomolecular Medicine, Faculty of Medicine and Health Sciences, Ghent University, De Pintelaan 185, 9000 Ghent, Belgium.
- <sup>c</sup> Department of Pharmaceutics, Faculty of Pharmaceutical Sciences, Ghent University, Harelbekestraat 72, 9000 Ghent, Belgium.
- <sup>d</sup> Tissue Engineering and Biomaterials Group, Department of Human Structure and Repair, Faculty of Medicine and Health Sciences, Ghent University, The Core, C. Heymanslaan 10, 9000 Ghent, Belgium.

### ARTICLE INFO

### Keywords: mRNA-lipid nanoparticles Cell-specific delivery Aminopeptidase N Nanobodies Apical-out intestinal organoids

### ABSTRACT

mRNA-based therapeutics formulated in lipid nanoparticles (mRNA-LNPs) have emerged as a groundbreaking platform technology for vaccination, immunotherapy, protein replacement therapy, and gene editing. However, a major bottleneck in their application is the lack of cell-specific delivery methods, which limits their efficacy and safety. To overcome this challenge, we developed a novel mRNA-LNP platform with targeted delivery capabilities. To this end, lipid nanoparticles were functionalized with nanobodies (VHH) specific to aminopeptidase N (APN), a cell surface protein on gut epithelial cells. These nanobodies were produced in genetically engineered *E. coli*, incorporating the non-canonical amino acid azido-phenylalanine into the VHH sequence to enable their precise conjugation onto lipid nanoparticles containing DSPE-PEG<sub>2000</sub>-TCO via a two-step click chemistry (SPAAC and IEDDA) reaction. Our findings demonstrate that APN-targeted, mRNA-loaded LNPs selectively target APN-expressing cells, enhancing LNP uptake and mRNA delivery to these cells. Furthermore, we show that directing the nanobody-functionalized mRNA-LNPs toward APN promotes their transcytosis across the gut epithelial barrier in porcine apical-out intestinal organoids and *in vivo*. Together, these findings highlight the potential of this programmable platform for the cell-specific delivery of mRNA-based vaccines and therapeutics. While this study focuses on porcine APN, the approach is adaptable across species, providing a versatile and customizable solution for the precise delivery of mRNA payloads to specific cells.

# 1. Introduction

Messenger RNA (mRNA) holds great promise for both prophylactic and therapeutic applications [1], including vaccines [2,3], protein replacement therapy [4], cancer immunotherapy [5,6], and gene editing using CRISPR-Cas9 [7]. Despite this potential, mRNA-based therapeutics face significant challenges due to their susceptibility to degradation [8]. To address these challenges, delivery vectors have been developed to protect mRNA from degradation and facilitate its delivery to the cytosol, thereby improving its therapeutic effectiveness [4,9]. Among the various delivery vectors, LNPs are preferred, as evidenced by the success of the COVID-19 mRNA vaccines from Pfizer/BioNTech (Comirnaty) and Moderna (Spikevax) [10]. These LNPs consist of four key components: ionizable cationic lipids (e.g., ALC-0315 or SM-102),

helper lipids (DSPC or DOPC), cholesterol, and polyethylene glycol lipids, like PEG<sub>2000</sub>-DMG [11,12]. Despite their success, mRNA-LNPs still face challenges, including accumulation at the injection site and the liver upon entering systemic circulation, as shown in pharmacokinetic studies of Pfizer's COVID-19 mRNA vaccine. The latter can lead to reversible liver damage and CD8+ T cell-mediated hepatitis, impacting both the efficacy and safety of the platform [13,14]. Designing strategies for targeted delivery of mRNA-LNPs could enhance their uptake by specific cells and further improve therapeutic outcomes [15].

Currently, two strategies are being investigated to achieve targeted delivery, including chemical modifications of LNPs and surface functionalization with affinity ligands. Chemical modifications have shown potential in preclinical studies for organ-specific mRNA delivery [16,17]. For instance, screening a library of lipids with modifications to

<sup>\*</sup> Corresponding author.

the head, tail, and linker regions identified lipid 113-O12B, enabling the selective delivery of LNPs to lymph nodes in mice, and facilitating their uptake by dendritic cells and macrophages [18]. Tissue-specific delivery can also be achieved by incorporating additional lipids, such as the cationic lipid DOTAP, into the LNP formulation, a strategy known as Selective Organ Targeting (SORT) [19]. This approach enables controlled biodistribution, allowing LNPs to preferentially accumulate in organs such as the lungs, spleen, or liver depending on their lipid composition [20]. SORT-LNPs, however, only target whole organs and cannot yet reach specific cell types or tissues like the gut [21]. In addition, their effectiveness might vary between species due to the deposition of a protein corona on the surface of the nanoparticles when they enter the body. The composition of this corona differs between humans and mice. While the latter contained more fibrinogen, the protein corona in humans had more immune-related proteins like immunoglobulins and complement C3 [22]. These differences can influence the interaction of nanoparticles with cells and imply that speciesspecific effects need to be considered when testing SORT-LNPs in

The second approach involves decorating the LNP surface with affinity ligands to achieve tissue- and or cell-specific delivery. A recent study demonstrated enhanced mRNA delivery to the placenta in pregnant mice by conjugating LNPs with epidermal growth factor receptor-specific antibodies using click chemistry [23]. Despite these promising results, Fc domains in monoclonal antibodies can activate complement pathways and Fc $\gamma$ R-expressing immune cells, potentially increasing immunogenicity and exacerbating inflammatory responses, which in turn increase the risk for immune-related pathologies [24]. These issues can be mitigated by mutating the Fc $\gamma$ R binding regions as well as by using F(ab')<sub>2</sub> fragments, scFv, single-domain antibodies (VHHs) or antibody-mimicking proteins (affibodies, DARPins) that lack Fc domains. VHHs offer advantages like a lower immunogenicity, smaller size, higher stability, and straightforward production as compared to conventional antibodies [25].

Cell type-specific delivery of LNPs could also facilitate mucosal administration of mRNA-based therapies. The gut epithelium presents a physical barrier that impedes the uptake of macromolecules and delivery vectors [26]. Targeting membrane proteins abundantly expressed on the apical surface of intestinal epithelial cells could improve the uptake of macromolecules [27]. For instance, the neonatal Fc receptor (FcRn) facilitates the transport of IgG or Fc domain-coated nanoparticles across the gut epithelium [28]. FcRn-targeted PLGA-PEG-Mal nanoparticles, functionalized with FcRn-specific affibodies via maleimidethiol conjugation, were successfully transported across the gut epithelium upon their injection in the lumen of human intestinal organoids [29]. Aminopeptidase N (APN) is another promising target to enhance transport across the gut epithelium. Our previous studies showed that targeting APN using conventional antibodies or VHHs increased the transport of vaccine antigens or yeast microparticles across the gut epithelium, eliciting strong immune responses that protected animals from infection [30-33]. Here, we leveraged our expertise and tools in APN targeting to functionalize LNPs with APN-specific VHHs using consecutive SPAAC (Strain-promoted Azide - Alkyne Click Chemistry reaction) and IEDDA (inverse electron demand Diels-Alder reaction) click chemistry. These VHHs were produced in E. coli strains, allowing the incorporation of an azido-phenylalanine to enable this click chemistry. We show that APN-targeted mRNA-loaded LNPs deliver their payload to specific cells and are transported across the intestinal epithelium in porcine apical-out small intestinal organoids and under in vivo conditions.

### 2. Materials & methods

# 2.1. Preparation and characterization of TCO-modified LNPs and DBCO-modified LNPs

The TCO-modified LNPs (TCO-LNPs) were synthesized by combining a lipid-containing ethanol phase with an mRNA-containing aqueous phase through vortexing for 30 s. The ethanol phase was formulated by dissolving ALC-0315 ((4-hydroxy butyl) azanediyl) bis (hexane-6,1-dial) bis (2-hexyl decanoate))(Sinopeg, Xiamen, Fujian, China), DSPC (1,2distearoyl-sn-glycero-3-phosphocholine)(Avanti Polar Lipids, Alabaster, Alabama, USA), Cholesterol (Sigma-Aldrich, Burlington, Massachusetts, USA), and DSPE-PEG<sub>2000</sub>-TCO (1,2-distearoyl-sn-glycero-3-phosphoethanolamine-N-(polyethyleneglycol)-TCO)(Ruixi Biological Technology, Xi'an, China) at molar ratios of 50:10:38.5:1.5 in ethanol. To assess how the DSPE-PEG<sub>2000</sub>-TCO content influences the uptake of APNtargeted VHH-LNPs, LNPs were prepared with varying ratios of DSPE-PEG<sub>2000</sub>-TCO and DMG-PEG<sub>2000</sub> while maintaining a total PEG-lipid content of 1.5 mol%. Three formulations were tested: 1.5 mol% DSPE-PEG<sub>2000</sub>-TCO, 1.0 mol% DSPE-PEG<sub>2000</sub>-TCO with 0.5 mol% DMG-PEG<sub>2000</sub>, and 0.5 mol% DSPE-PEG<sub>2000</sub>-TCO with 1.0 mol% DMG-PEG<sub>2000</sub>. All formulations contained identical core lipid compositions (ALC-0315, DSPC, cholesterol). To generate DBCO-modified LNPs (DBCO-LNPs), DSPE-PEG2000-TCO was substituted with DSPE-PEG2000-DBCO (Avanti Polar Lipids, USA) at the same molar percentage (1.5 %). For Cy5-labeled formulations, 0.1 mol% of DSPC was replaced by DSPC-Cy5 (Avanti Polar Lipids). To formulate DiD-labeled LNPs, 0.1 mol% of DSPC was substituted with DiD (lumiprobe, USA). The aqueous phase was established in 5 mM acetate buffer (pH 4.0) (Sigma-Aldrich), containing eGFP encoding mRNA (Cellerna Bioscience, Baesweiler, Germany) at varying concentrations. They were mixed in a 2:1 ( $\nu/\nu$ ) ratio to homogenize the aqueous and ethanol phases and vortexed vigorously. The resulting LNPs were dialyzed against ultra-pure water using 12,000 MWCO cassettes (Thermo Fisher Scientific, Waltham, Massachusetts, USA) at 25 °C for 3 h to remove ethanol and unencapsulated components. The mean particle size (Z-average diameter), polydispersity index (PDI), and zeta-potential of TCO-LNPs were measured in 5 mM HEPES buffer (pH 7.4) with a Zetasizer Nano ZS (Malvern Instruments, UK) equipped with a HeNe laser ( $\lambda = 633$  nm) and detected at a scattering angle of 173°.

The encapsulation efficiency of mRNA in TCO-LNPs was quantified using a modified Quant-iT<sup>TM</sup> RiboGreen RNA Assay (Invitrogen, Waltham, Massachusetts, USA). Following encapsulation, mRNA in the supernatant (unencapsulated mRNA, OD $_{\rm unencapsulated}$ ) and in the LNPs (total mRNA, OD $_{\rm total}$ ) was quantified. For the latter, LNPs were lysed with Triton-X to release the encapsulated mRNA. The encapsulation efficiency was calculated using the formula:

$$\textit{Encapsulation Efficiency}(\%) = \frac{\left(\textit{OD}_{\textit{total}} - \textit{OD}_{\textit{unencaptulatred}}\right)}{\textit{OD}_{\textit{total}}} \times 100\%$$

# 2.2. Production of single-domain antibodies carrying an azidophenylalanine

Para-azidophenylalanine (pAzF)-modified single domain antibodies, hereafter referred to as VHH-AzF, were engineered by introducing a pAzF residue at the carboxyl terminus of the VHH primary structure [34]. This was achieved by genetically incorporating an amber stop codon (TAG) at the C-terminus of both the APN-specific ( $\alpha$ APN-VHH, clone 3 L73) [33] and mCherry-specific (Ctrl-VHH) VHH sequence (clone LaM2; accession number 7SAJ). The integration of pAzF at the amber stop codon within the VHH sequences was facilitated by using the appropriate tRNA/tRNA synthetase orthogonal pair (pEVOL-pAzF, Addgene Plasmid #31186). These constructs were cloned into the pET22 vector (performed by Genscript, China) and co-transformed with pEVOL-pAzF into *E. coli* WK6 cells through electroporation. The

transformants were then transferred to a selective TB medium supplemented with 1 mM pAzF (abcr, Karlsruhe, Germany) and grown until they reached an  $OD_{600}$  of 0.5. At this point, 0.2 % (w/v) arabinose (Sigma-Aldrich, Massachusetts, USA) was added for induction. When the cultures reached an OD<sub>600</sub> of 0.8, induction was further enhanced with 1 mM IPTG (Biosynth, Staad, Switzerland). The bacteria were cultured overnight at 28 °C and subsequently harvested by centrifugation at 13,500 ×g for 30 min. Cells were then lysed using a French Press G-M® High-Pressure Cell Disruption system (Glen Mills, New Jersey, USA), followed by short sonication. Supernatants were collected following centrifugation at 13,500  $\times g$  for 30 min. Subsequently, the VHHs were purified through Immobilized Metal Affinity Chromatography (IMAC) using Talon® beads (Takara, Kusatsu, Japan) and eluted with 250 mM imidazole (Sigma). The remaining impurities were removed by size exclusion on an ÄKTA pure<sup>TM</sup> chromatography system (Cytiva, Marlborough, USA). The obtained αAPN-VHH-AzF and Ctrl-VHH-AzF single domain antibodies were dialyzed overnight at 4  $^{\circ}$ C against HEPES buffer (50 mM HEPES-Na, 50 mM NaCl, pH 7.4) to enable the subsequent click reactions. Protein concentrations were measured by BCA (Bio-rad, California, USA) following the manufacturer's instructions.

#### 2.3. SDS-PAGE and western blotting

The purity of the modified VHHs was assessed via SDS-PAGE and western blotting. For SDS-PAGE, 5 µg of each sample was loaded and separated using a 15 % gel, followed by staining with Coomassie Blue PhastGel® (GE Healthcare, Chicago, USA) to visualize protein bands.

After electrophoresis, the proteins were transferred to a PVDF membrane (Cytiva, Marlborough, USA) using a Trans-Blot Turbo Transfer System (Bio-Rad). The membrane was then blocked overnight at 4 °C in a blocking buffer (PBS, 0.2 % Tween 20 (Sigma-Aldrich) and 5 % skim milk (Regilit, Bourgogne, France)). For immunodetection, the blocked membrane was incubated with a monoclonal rabbit anticamelid VHH antibody (1:1000 dilution in blocking buffer, Genscript, cat. A01860–200) overnight at 4 °C. Following three washes with PBS containing 0.2 % Tween 20, the membrane was incubated at room temperature with HRP-conjugated polyclonal swine anti-rabbit IgG (1:2000 dilution in blocking buffer, Dako, Glostrup, Denmark, cat. 41,456,526). Finally, protein bands were visualized using the Super-Signal<sup>TM</sup> West Pico PLUS Chemiluminescent Substrate (Thermo Scientific, Massachusetts, USA) and imaged with a ChemiDoc MP system (Bio-Rad).

# 2.4. Functionalization of LNPs with single domain antibodies using click reaction

To verify the successful incorporation of para-azido-phenylalanine (pAzF), αAPN-VHH-AzF and control-VHH-AzF were labeled with Alexa Fluor 488 (AF488) via both one-step and two-step click chemistry. For the one-step SPAAC reaction, DBCO-AF488 (baseclick GmbH, Munich, Germany) was directly added to VHH-AzFs in HEPES buffer (50 mM HEPES-Na, 50 mM NaCl, pH 7.4) at a 10:1 M ratio. The mixture was incubated at 37 °C with shaking (200 rpm) for 2 h to allow for strainpromoted azide-alkyne cycloaddition. For two-step click, VHH-AzFs were first incubated with sulfo-6-methyl-tetrazine-DBCO (DBCO-Tetrazine) (Bio-Connect, Huissen, the Netherlands) to generate intermediates and then with a trans-cycloalkene-functionalized AlexaFluor 488 (AF488-TCO) (Click Chemistry Tool, Scottsdale, AZ). Specifically, this involved 2 h of the Strain-Promoted Azide-Alkyne Cycloaddition reaction (SPAAC) of VHH-AzF's cycloalkyne with DBCO-Tetrazine and 1 h of the ultra-fast inverse electron demand Diels-Alder reaction (IEDDA) of the tetrazines with AF488-TCO in HEPES buffer (50 mM HEPES-Na, 50 mM NaCl, pH 7.4) at 37  $^{\circ}$ C, with shaking at 200 rpm. To shift the chemical equilibrium toward the product (VHH-AF488) and enhance the reaction efficiency, we added a slight excess of DBCO-Tz or AF488-TCO at each step. From preliminary data, the optimal molar ratios of  $\alpha APN\text{-}VHH\text{-}AzF\text{:}DBCO\text{-}Tz\text{:}$  AF488-TCO were determined as 1:5:10. The resulting  $\alpha APN\text{-}VHH\text{-}AF488$  and ctrl-VHH-AF488 were loaded (0.5  $\mu g$  and 2  $\mu g)$  on SDS-PAGE (10 %) and visualized using a Coomassie stain and fluorochrome detection using a ChemiDoc MP (Bio-Rad).

To functionalize TCO-LNPs with VHHs, two reaction sequences were evaluated. In the first approach, 10 µM VHH-AzF was conjugated to 50 μM DBCO-Tetrazine via SPAAC chemistry in 50 mM HEPES buffer at 37 °C with shaking (200 rpm) for 2 h. The resulting VHH-Tetrazine was then conjugated to TCO-LNPs at molar ratios of 1:10 or 2:10 for 1 h at 37 °C with shaking using IEDDA chemistry. In the second approach, 50  $\mu M$  DBCO-Tetrazine was conjugated to 10  $\mu M$  TCO-LNPs via IEDDA chemistry for 1 h at 37  $^{\circ}\text{C}$  with shaking. The resulting DBCO-LNPs were then functionalized with VHH-AzF via SPAAC chemistry at molar ratios of 1:10 or 2:10 by 1 h incubation at 37  $^{\circ}$ C with shaking (200 rpm). To functionalize DBCO-LNPs directly, VHH-AzF was incubated with DBCO-LNPs at a molar ratio of 2:10 using SPAAC chemistry for 1 h at 37 °C with shaking (200 rpm). In all cases, excess reactants were used to shift the equilibrium toward VHH-LNP formation. Unreacted components were removed using Amicon Ultra-0.5 Centrifugal Filter Units (50 kDa MWCO; Sigma-Aldrich). The efficiency of the click reactions to generate VHH-LNPs was evaluated by SDS-PAGE (10 %), with 10 µL of VHH-LNPs loaded per lane.

# 2.5. Cell lines

Baby Hamster Kidney (BHK) cells and APN-expressing BHK cells (BHK-APN) were maintained in Dulbecco's minimum essential medium (DMEM)(Gibco) supplemented with 5 % ( $\nu/\nu$ ) fetal bovine serum (FBS, Invivo),  $100\,\mathrm{U\,mL^{-1}}$  penicillin (Life Technologies),  $100\,\mathrm{\mu g\,mL^{-1}}$  streptomycin(Life Technologies), 1 % ( $\nu/\nu$ ) Non-essential Amino Acids Solution (NEAA, Life Technologies, California, USA), 1 mM ( $\nu/\nu$ ) Sodium Pyruvate (Life Technologies), and 1 mM  $\nu$ -glutamine (Life Technologies). The porcine small intestinal epithelial cell line IPEC-J2-APN was maintained in DMEM-F12 (Gibco, California, USA) supplemented with 5 % FBS,  $100\,\mathrm{U\,mL^{-1}}$  penicillin,  $100\,\mathrm{\mu g\,mL^{-1}}$  streptomycin, 2 %  $\nu$ -glutamine (Life Technologies), and 1 % ITS Liquid Media Supplement (Sigma-Aldrich). The cell lines were maintained in a humidified incubator at  $37\,\mathrm{^{\circ}C}$ ,  $5\,\mathrm{^{\circ}CO_2}$ . Cells were passaged using trypsin solution ( $0.25\,\mathrm{^{\circ}M}$  Trypsin (ThermoFisher),  $100\,\mathrm{U\,mL^{-1}}$  penicillin,  $100\,\mathrm{\mu g\,mL^{-1}}$  streptomycin, and  $0.53\,\mathrm{mM}$  EDTA (VWR, Pennsylvania, USA)).

## 2.6. Enteroid cultures

Small intestinal crypts were isolated from 3- to 6-week-old piglets [35]. After euthanasia, the abdominal cavity was opened, and sections (10 cm) of the duodenum, jejunum without Peyer's patches, and ileum were isolated and immediately put in ice-cold, sterile PBS. The ileal tissue was processed to remove the Peyer's patches. Upon washing in PBS supplemented with 100 U/mL penicillin and 100 µg/mL streptomycin, the intestinal tissues were incubated in ice-cold dissociation buffer 1 (30 mM EDTA, VWR), 1.5 mM dithiothreitol (Sigma), 6 μM Rhoassociated kinase (ROCK) inhibitor (Y-27632; Sigma) in PBS) for 30 min on ice on an orbital shaker. Every 5 min, the tissues were shaken vigorously for 10-15 s. After 30 min, the tissues were transferred to dissociation buffer 2 (30 mM EDTA, 6  $\mu M$  Y-27632 in PBS, 37  $^{\circ} C)$  and incubated for 10 min on an orbital shaker. Following a final wash in cold, sterile PBS with increased shaking frequency (every 2 min), single crypts were isolated and counted. Crypts were then resuspended in icecold growth factor-reduced Cultrex<sup>TM</sup> (R&D Systems, Minnesota, USA), supplemented with 5 % ( $\nu/\nu$ ) human IntestiCult<sup>TM</sup> Organoid Growth Medium (STEMCELL Technologies, Vancouver, Canada), and 0.5 % ( $\nu/$  $\nu$ ) Y-27632 (Sigma). A 40  $\mu$ L Cultrex droplet containing 75 crypts was placed onto a pre-warmed (37  $^{\circ}\text{C})$  24-well plate. The plates were then incubated at 37  $^{\circ}\text{C}$  for 15 min to polymerize the Cultrex. Subsequently, 350 µL of IntestiCult<sup>TM</sup> Organoid Growth Medium, supplemented with 100 U/mL penicillin (Sigma) and 100 μg/mL streptomycin (Sigma), was

added. The crypts were maintained in a humidified incubator at 37  $^{\circ}$ C with 5  $^{\circ}$ CO<sub>2</sub>, and the medium was replaced every 2 days until passaging.

To passage the enteroids, Cultrex domes were washed once with cold DPBS (Gibco), and 0.5 mL cold cell recovery solution (Corning, USA) was added forcefully to break up the dome. After a 30 min incubation on ice, enteroids were collected, centrifuged (200  $\times g$ , 5 min, 4 °C), and resuspended in 1 mL cold DPBS with 10  $\mu M$  Y-27632. A 1 mL syringe and a 27-gauge needle (Terumo, Leuven, Belgium) were used to fragment the enteroids through 2 to 3 aspirations (4 times for the monolayer culture). The fragments were then collected by centrifugation (200  $\times g$ , 5 min, 4 °C), resuspended in 40  $\mu L$  Cultrex, and cultured as described above.

To obtain 2D monolayers, enteroid fragments were resuspended in 400  $\mu$ L pre-warmed IntestiCult<sup>TM</sup> Organoid Growth Medium (human) and plated on 24-well plates with glass inserts, which were coated with 2.5  $\mu$ g/cm² collagen IV (mouse, Corning). After 2 days, cell cultures were washed with DPBS, and 400  $\mu$ L complete IntestiCult<sup>TM</sup> Organoid Differentiation Medium (human) was added. Confluence was achieved after 2–3 days.

To generate apical-out enteroids [36], enteroid fragments were collected through centrifugation (200  $\times$ *g*, 5 min, 4 °C), resuspended in 400  $\mu$ L pre-warmed (37 °C) IntestiCult<sup>TM</sup> Organoid Growth Medium (human, StemCell Technologies) in a 24-well ultra-low attachment surface plate (Corning) and maintained in a humidified incubator at 37 °C with 5 % CO<sub>2</sub>. After 2–3 days, enteroids were centrifuged (200  $\times$ *g*, 5 min, 4 °C) and resuspended in 400  $\mu$ L pre-warmed IntestiCult<sup>TM</sup> Organoid Differentiation Medium (human, StemCell Technologies). The enteroids were kept under the same conditions for 2 to 3 days.

# 2.7. Verification of apical-out topology and APN expression in Enteroid cultures

To verify the apical-out topology of the enteroids and detect APN expression in apical-out enteroids and enteroid monolayers, samples were fixed with 4 % paraformaldehyde (PFA) at room temperature (RT) for 10 min. Samples were incubated with an APN-specific VHH (clone 3 L73) fused to the Fc domain of mouse IgG2a (produced in-house) and a control monoclonal antibody (anti-FedF, mouse IgG2a, clone 19F6, inhouse), both at 2.5  $\mu$ g/mL in DPBS (Gibco), for 1 h at 4  $^{\circ}$ C. After two DPBS washes, goat anti-mouse IgG2a-AF488 (1:200 dilution in DPBS, Invitrogen, cat. A21131) was added, and the samples were incubated for 30 min at 4 °C. Following APN staining, the actin cytoskeleton was stained using TexasRed-X Phalloidin (1:200 dilution in DPBS; Thermo Scientific, cat. 2,795,231) to verify apical-out topology of the enteroids, while Hoechst 33342 (10 μg/mL, Invitrogen) was added to stain nuclei. The samples were incubated for 10 min at RT. After two washes with DPBS, enteroid monolayers were mounted using an anti-fading solution (DABCO, Sigma-Aldrich) and imaged using a Leica LAS AF Lite confocal microscope. For apical-out enteroids, samples were washed twice with DPBS, resuspended in 200 µL DPBS, and transferred to chamber slides (ibidi, Gräfelfing, Germany). Imaging was performed with a Stellaris 8 Falcon confocal microscope (Leica Microsystems) as described previously [37].

# 2.8. Assessment of APN binding by fluorescently labeled single domain antibodies

To determine whether the one-step or two-step click conjugation affects the target binding of  $\alpha APN\text{-}VHH\text{-}AF488,$  flow cytometry was used to assess its interaction with APN-expressing cells. BHK-APN cells and parental BHK cells (negative control) were seeded in 96-well V-bottom plates at 20,000 cells per well. After 24 h, cells were washed with staining buffer (RPMI-1640 + 1 % FBS), and 0.7  $\mu M$   $\alpha APN\text{-}VHH\text{-}AF488,$  generated via either one-step or two-step click chemistry, was added in 100  $\mu L$  of PBS. The cells were resuspended and incubated on ice for 30

min, followed by three washes with ice-cold PBS. Subsequently, cells were resuspended in PBS-EDTA (1 mM) and analyzed with a Cytoflex flow cytometer (Beckman Coulter, Brea, California, USA). The ctrl-VHH-AF488 was used as an isotype control, while  $\alpha APN-VHH-Fc\ mIgG2a$  (inhouse), detected by an AF488-labeled anti-camelid VHH Ab (1:500 dilution in staining buffer, Genscript, cat. A01862–200), was used as a positive control.

# 2.9. Comparison of one-step and two-step click chemistry for $\alpha APN\text{-}VHH\text{-}LNP$ functionalization

Following successful validation of  $\alpha APN-VHH-AzF$  labeling using both one-step (DBCO-AF488) and two-step (DBCO-tetrazine + AF488-TCO) click chemistry, we applied the same strategies to conjugate  $\alpha APN-VHH-AzF$  to LNPs modified with DBCO or TCO. Ctrl-VHH-LNPs and unmodified DBCO-LNPs were included as negative controls.

To evaluate LNPs uptake and mRNA translation efficiency, BHK-APN cells were seeded in flat-bottom 96-well plates (Greiner Bio-One, Austria) at 20,000 cells per well. Cells were incubated with 2.5  $\mu L$  of Cy5-labeled LNPs ( $\alpha$ APN-VHH-LNP, Ctrl-VHH-LNP, or DBCO-LNP, each encapsulating 100 ng/ $\mu L$  eGFP mRNA) diluted in 50  $\mu L$  Opti-MEM for 30 min at 37 °C. After this preincubation, 50  $\mu L$  of complete BHK medium (pre-warmed to 37 °C) was added, and cells were cultured for 24 h at 37 °C with 5 % CO2. Post-incubation, cells were detached using trypsin, washed, and analyzed by flow cytometry (Cytoflex). Cy5 fluorescence was used to assess LNP uptake, and GFP expression indicated mRNA delivery and translation.

### 2.10. Assessment of APN binding of the VHH-functionalized LNPs

An ELISA was conducted to ascertain whether the VHHfunctionalized LNPs could bind to APN. Specifically, 96-well MaxiSorp<sup>TM</sup> ELISA Plates (Thermo Scientific) were coated with 100  $\mu L$  (10 μg/mL) of porcine APN (Sigma) per well overnight at 4 °C. The plates were then blocked with 250 µL/well of blocking buffer (PBS containing 3 % BSA (MP biomedicals, California, USA)) and incubated for 2 h at 37 °C. Upon blocking, a twofold dilution series of  $\alpha APN\text{-}VHH\text{-}LNPs$  and unconjugated TCO-LNPs ranging from 2<sup>2</sup> to 2<sup>9</sup> were prepared in PBS with 3 % BSA (dilution buffer). An equivalent concentration of  $\alpha APN$ -VHH-AzF was added as a negative control, while plates only coated with APN served as blanks. Subsequently, a 100 µL sample was added to the plates and incubated for 1 h at 37  $^{\circ}$ C. Following this, 100  $\mu$ L biotinylated APN (10 ug/mL) in dilution buffer was added and incubated for 1 h hour at 37 °C. Next, 100 µL Streptavidin-HRP (1:1000 in dilution buffer, R&D systems) was added and incubated for 1 h at 37 °C. The plate was washed four times with PBS between each incubation step. Then, 50 µL ABTS substrate was added and incubated for 30 min at 37 °C. The absorbance was measured at 405 nm using a Spectra Fluor (TECAN, Männedorf, Switzerland).

# 2.11. Binding to and uptake of APN-targeted VHH-LNPs by an APN-expressing cell line

To assess the APN-mediated cell binding and uptake of  $\alpha$ APN-VHH-LNPs, BHK and BHK-APN cells were seeded at 20,000 cells per well in a sterile conical bottomed 96-well plate (Thermo Scientific). They were then incubated with 2.5 µL Cy5-labeled  $\alpha$ APN-VHH-LNPs in 100 µL cold Opti-MEM medium (Gibco) for 1 h at 4 °C. Unbound LNPs were removed by centrifugation (400 ×g, 5 min, 4 °C) and washed twice with PBS. The cells were subsequently transferred into 96-well cell culture plates (VWR) in 100 µL/well cell culture medium and incubated for 4, 24, and 48 h at 37 °C, 5 % CO<sub>2</sub>. After the respective incubation periods, the cells were trypsinized, resuspended in ice-cold PBS-EDTA (1 mM), and analyzed using flow cytometry (Cytoflex). Confocal microscopy was used to confirm the uptake of LNPs by the cells. Unbound  $\alpha$ APN-VHH-LNPs were removed, and the cells were washed twice with DPBS (Gibco)

in a conical-bottom 96-well plate via centrifugation. The washed cells were then transferred to 24-well culture plates (Greiner bio-one, Kremsmünster, Austria) containing glass coverslips (Epredia, Braunschweig, Germany), with a transfer ratio of three 96-well cells to one 24-well well. Each well contained 300  $\mu L$  of cell culture medium, and the cells were incubated for 24 h at 37  $^{\circ} C$ , 5 % CO $_2$ . After incubation, the cells were washed twice with DPBS at room temperature (RT) to remove unattached dead cells. They were then fixed with 4 % PFA for 10 min at RT. Hoechst 33342 (10  $\mu g/m L$ , Invitrogen) was added for nuclear staining, followed by two additional DPBS washes. Finally, the coverslips were mounted onto slides, and confocal microscopy (Leica LAS AF Lite) was performed to visualize the LNPs inside the cells.

# 2.12. Assessment of LNP cytotoxicity

To assess whether LNPs influence cell viability, varying amounts of VHH-LNPs (1  $\mu$ L, 2.5  $\mu$ L, and 5  $\mu$ L), corresponding to mRNA concentrations of 100 ng, 250 ng, and 500 ng, were added to 20,000 cells (BHK, BHK-APN, and IPEC-J2-APN) per well in 100  $\mu$ L of cell culture medium. The cells were seeded in a flat-bottom 96-well plate (Greiner Bio-One, Kremsmünster, Austria) and incubated with the LNPs for 24 and 48 h at 37 °C, 5 % CO<sub>2</sub>. Upon incubation, the cells were detached with trypsin buffer, stained with the live/dead cell marker Sytox blue (1:1000 dilution, cat.2585788, Invitrogen), and measured using flow cytometry (Cytoflex, Beckman Coulter). Data were analyzed using CytExpert 2.4 software (Beckman Coulter, Brea, California, US) and FlowJo<sup>TM</sup> v10.9 Software (Ashland, Oregon).

# 2.13. APN-mediated delivery of mRNA to APN-expressing cells by APN-targeted VHH-LNPs

To assess whether APN-mediated LNP internalization can successfully deliver and translate mRNA, the APN-expressing cell lines BHK-APN and IPEC-J2-APN were used. Cells were detached and seeded at 20,000 cells per well in a flat-bottomed 96-well plate (Greiner Bio-One, Kremsmünster, Austria). They were incubated with 1  $\mu$ L, 2.5  $\mu$ L, or 5  $\mu$ L of Cy5-labeled LNPs (including DBCO-LNP,  $\alpha$ APN-VHH-LNP, and Ctrl-VHH-LNP, each encapsulating 100 ng/ $\mu$ L eGFP mRNA) in 50  $\mu$ L of Opti-MEM medium for 30 min at 37 °C. Next, 50  $\mu$ L of pre-warmed (37 °C) complete culture medium was added, and cells were incubated for 24 h at 37 °C, 5 % CO<sub>2</sub>. Following incubation, cells were trypsinized, and Cy5 and GFP fluorescence intensities were measured by flow cytometry (Cytoflex).

To further distinguish APN-specific binding from non-specific interactions, BHK-APN cells were detached and seeded at 20,000 cells per well in a conical-bottom 96-well plate (Nunc, Sjelland, Denmark). Cells were incubated with 2.5  $\mu L$  of Cy5-labeled LNPs (including DBCO-LNP,  $\alpha$ APN-VHH-LNP, and Ctrl-VHH-LNP, each encapsulating 100 ng/ $\mu L$  eGFP mRNA) in 50  $\mu L$  of cold Opti-MEM medium for 30 min on ice. After incubation, cells were washed three times with cold PBS containing 1 % fetal bovine serum (FBS, Invivo) by centrifugation at 400 g for 5 min at 4 °C to remove unbound LNPs. The cells were then resuspended in 100  $\mu L$  of pre-warmed (37 °C) complete culture medium and transferred to a flat-bottomed 96-well plate (Greiner Bio-One, Kremsmünster, Austria). Cells were incubated for 24 h at 37 °C, 5 % CO<sub>2</sub>, then trypsinized, and Cy5 and GFP fluorescence intensities were measured using flow cytometry (Cytoflex).

To evaluate how the DSPE-PEG $_{2000}$ -TCO content in the LNPs affected their uptake and mRNA delivery, TCO-LNPs containing different ratios of DSPE-PEG $_{2000}$ -TCO and DMG-PEG $_{2000}$  (Section 2.1) were functionalized with VHHs via the two-step click chemistry reaction described above. VHH-functionalized LNPs or DBCO-LNPs were added to BHK-APN cells for 24 h at 37  $^{\circ}$ C under 5  $^{\circ}$ C CO<sub>2</sub>. After incubation, cells were washed three times with PBS to remove unbound nanoparticles, trypisinized and LNP internalization (Cy5 channel) and mRNA delivery efficiency (GFP channel) were measured with flow cytometry.

For immunofluorescence staining, BHK-APN and IPEC-J2-APN cells were seeded at 60,000 cells per well into 24-well culture plates (Greiner bio-one), containing cover glass slips (epredia), and 7.5  $\mu L$  LNPs were added, corresponding to an mRNA concentration of 750 ng, in 180  $\mu L$  Opti-MEM and 180  $\mu L$  complete medium. The cells were subsequently incubated for 24 h at 37 °C, 5 % CO<sub>2</sub>. Following incubation, the medium was discarded, cells were washed twice with DPBS(Gibco), and fixed with ice-cold 70 % ethanol at -20 °C. After a 10 min fixation period, cells were washed with PBS, stained with Hoechst 33342(10  $\mu g/mL$ ; Invitrogen) at RT for 5 min, washed twice, and mounted with anti-fading solution Dabco mounting (Sigma-Aldrich). Imaging was performed using confocal microscopy (Leica LAS AF Lite).

# 2.14. Analysis of endosomal acidification upon LNP internalization

To assess endosomal acidification,  $\alpha APN\text{-VHH-AzF}$  and Ctrl-VHH-AzF were labeled with pHrodo<sup>TM</sup> Green AM Intracellular pH Indicator Dyes (ThermoFisher) following the manufacturer's instructions. Subsequently, a 2-step click reaction was used to decorate the surface of the LNPs with pHrodo<sup>TM</sup> Green-labeled  $\alpha APN\text{-VHH-LNP}$  and Ctrl-VHH-LNP as described above. BHK-APN cells and IPEC-J2-APN cells were trypsinized and seeded in 96-well plates at a density of 25,000 cells per well, incubated with 2.5  $\mu$ L of each LNPs in 50  $\mu$ L Opti-MEM (for BHK-APN cells) and 50  $\mu$ L DMEM-F12 (for IPEC-J2-APN cells) at 4 °C for 1 h. After incubation, the non-binding LNPs were washed away through centrifugation (400  $\times$ g, 5 min, 4 °C), and the cells were resuspended in 100  $\mu$ L warm complete medium, transferred to a 96-well plate, and incubated for 4 h and 24 h at 37 °C, 5 % CO<sub>2</sub>. Cy5 and pHrodo fluorescence intensity were measured at 4 h (37 °C) and 24 h (37 °C) using flow cytometry (Cytoflex).

# 2.15. Internalization of VHH-LNPs by primary intestinal epithelial cells

The internalization of VHH-LNPs was evaluated in 3D (apical-out) enteroids and 2D enteroid monolayers. Following the described formulation process, apical-out enteroids were collected in Eppendorf tubes, centrifuged at 200  $\times g$  for 5 min at 4 °C, and the supernatant was carefully removed. The culture medium overlaying the enteroid monolayers was aspirated to prepare them for subsequent analysis. Subsequently, 7.5  $\mu L$  of each LNP (containing 750 ng mRNA) in 400  $\mu L$ complete IntestiCult<sup>TM</sup> Organoid Differentiation Medium (Human) was added to the monolayers or apical-out enteroids and incubated for 48 h. Following this incubation, monolayers were fixed using 4 % PFA (RT, 15 min) and mounted with anti-fading solution (DABCO, Sigma-Aldrich) and imaged using confocal microscopy (Leica LAS AF Lite). In contrast, live apical-out enteroids were resuspended in 200 µL imaging medium (DMEM (Sigma, D5030), 10 mM D-glucose, 10 mM HEPES, 1 mM sodium pyruvate, 2 mM Glutamax) in chamber slides (ibidi, Gräfelfing, Germany) and imaged with a Stellaris 8 Falcon confocal microscope (Leica Microsystems)(see supplementary data for detailed microscope settings). To evaluate the transport efficiency of APNtargeted LNPs, maximum intensity projection (MIP) z-stack images were analyzed. Regions of interest (ROIs) were selected, and the mean fluorescence intensity (MFI) within each ROI was quantified using Leica LAS X software (version 5.2.2).

# 2.16. Gut-ligated loop experiments

To assess the in vivo behaviour of the APN-targeted mRNA-LNPs in the small intestine, a gut ligated loop experiment was performed as approved by the Ethical Committee of the Faculties of Veterinary Medicine and Bioscience Engineering at Ghent University, following the Belgian law on animal experimentation (EC2024/038). Three piglets (female, 5 weeks old) were acclimated for one week, fasted overnight with access to water, and anesthetized with ketamine (10 mg/kg) and xylazine (2 mg/kg), followed by maintenance under 2–3 % isoflurane in

oxygen. A midline laparotomy was performed to expose the jejunum, and four ligated loops (4 cm) were surgically created in each animal, spaced 10 cm apart, carefully avoiding Peyer's patches. The blood supply to each loop was maintained by placing ligatures between the mesenteric arcades. In the lumen of the gut loops, 900  $\mu L$  of DiD-labeled LNPs containing 90 µg mEGFP mRNA and diluted in HEPES buffer (50 mM HEPES, 50 mM NaCl, pH 7.3) to obtain a total volume of 3.5 mL was injected. Four formulations were tested: aAPN-VHH-LNPs, Ctrl-VHH-LNPs, DBCO-LNPs, and HEPES buffer alone (negative control). Upon injection, the gut loops were gently repositioned in the abdominal cavity, and the incision was closed. Animals remained under anesthesia during the 6 h incubation period. Following incubation, animals were euthanized by intravenous injection of 20 % sodium pentobarbital (60 mg/2.5 kg; Kela). The gut loops and draining MLNs were excised, rinsed three times with ice-cold DPBS (Gibco) to remove residual luminal content, and kept on ice and protected from light. Tissues were embedded in 2 % Methocel® MC (Fluka), snap-frozen in liquid nitrogen, and stored at -80 °C for further analysis.

# 2.17. Confocal microscopy on intestinal tissues

To visualize LNP distribution and mRNA translation within small intestinal tissues and MLN, cryosections (10  $\mu m$ ) were made using a Leica CM3050 S cryostat at  $-20~^{\circ}\text{C}$ . Sections were mounted on APES-coated glass slides (Paul Marienfeld GmbH & Co. KG, Lauda-Königshofen, Germany). Slides were air-dried at RT for 30 min and fixed in 4 % PFA for 15 min at RT. Sections were then washed three times for 5 min in DPBS (Gibco). Nuclei were stained with Hoechst 33342 (10  $\mu g/$  mL) (Thermo Fisher) for 10 min at RT, followed by three additional washes in DPBS. Slides were mounted in glycerol (Fisher Scientific) containing DABCO (Sigma-Aldrich) to prevent photobleaching.

Confocal microscopy imaging was performed on these sections using a Leica LAS AF Lite confocal microscope(ACS APO  $10.0 \times 0.30$  DRY, ACS APO  $20.0 \times 0.60$  IMM objectives). For each tissue, two sections spaced at least 0.5 cm apart were selected, and two representative fields per section were imaged and analyzed. Fluorescence intensity in the DiD (LNP internalization) and GFP (mRNA translation) channels was quantified using ImageJ software (National Institutes of Health, Bethesda, MD, USA), measuring the integrated density (IntDen = area  $\times$  mean value) for each image.

# 2.18. Data analyses

Statistical analyses were performed using GraphPad Prism version 10 (GraphPad Software Inc., San Diego, CA, USA). Normality of the data was assessed using the Shapiro–Wilk test ( $\alpha=0.05$ ), and all datasets passed. Homogeneity of variances was evaluated using the Brown–Forsythe test. Datasets with equal variances ( $P \geq 0.05$ ) were analyzed using one-way ANOVA followed by Holm–Šídák post hoc tests. For datasets with unequal variances (P < 0.05),  $\log_{10}$  transformation was applied; homogeneity was achieved post-transformation, and the data were then analyzed using one-way ANOVA with Holm–Šídák post hoc tests.

## 3. Results

# 3.1. Functionalization of LNPs with single-domain antibodies

To enable cell-specific delivery of LNPs, we wanted to decorate the surface of the LNPs with single-domain antibodies or VHHs. Due to their small size, we reasoned that cellular uptake of the functionalized LNPs would not be hampered. To facilitate the surface decoration of the LNPs with the VHHs, click chemistry was chosen. This requires the presence of a functional group in the VHH sequence. To avoid using functional groups in the antigen-binding domain of the VHHs, we opted to add this functional group at the C-terminus. To this end, a genetically engineered

*E. coli* strain in which all amber stop codons (TAG) are replaced with other stop codons was used [38]. This allows to use of the amber stop codon to encode non-canonical amino acids. Consequently, we synthesized a VHH DNA sequence with an amber stop codon at the C-terminus of the single domain antibodies (Fig. 1a). Transformation of *E. coli* with a plasmid encoding the VHH construct, along with a plasmid for the tRNA/tRNA synthetase orthogonal pair responsible for incorporating the non-canonical amino acid para-azidophenylalanine (AzF) at amber stop codons, resulted in successful VHH production (Fig. 1b). This method yielded approximately 10 to 20 mg of VHH per liter of culture medium.

To confirm successful AzF incorporation, we conjugated the fluorochrome reporter DBCO-AlexaFluor488 to VHH-AzF using a strain-promoted azide–alkyne cycloaddition (SPAAC) one-step click chemistry reaction (Fig. 1c). This resulted in fluorescently labeled APN-specific VHH-AzF and Ctrl-VHH-AzF, as confirmed by SDS-PAGE and in-gel fluorescence (Fig. 1d), indicating that AzF incorporation was successful. Next, we sought to verify whether incorporating the pAzF moiety did not compromise the binding of the VHHs to APN. Flow cytometry showed that both one-step and two-step generated  $\alpha$ APN-VHH-AF488 can bind to BHK-APN cells, while, as expected, Ctrl-VHH-AF488 did not (Fig. 1e). Together, these results indicate that the modified VHHs can be used to decorate the surface of LNPs via click chemistry.

To functionalize LNPs with VHH-AzF, we used DBCO-modified LNPs to conjugate VHH-AzF in a one-step click reaction. However, we consistently observed a severe and irreversible aggregation of the LNPs upon functionalisation with the VHHs (Fig. 2a). Since these aggregates severely affect APN targeting efficiency and mRNA delivery ability of LNPs on BHK-APN cells (Fig. S1a,b), we adopted a two-step click reaction strategy using TCO-LNPs and a soluble DBCO-tetrazine (Tz) intermediate. Before applying this strategy to LNPs, we first validated it using  $\alpha$ APN-VHH-AzF and TCO-AF488 as a fluorescent probe (**Fig. S2a**). The reaction successfully produced fluorescently labeled  $\alpha APN-VHH$ -AF488, as confirmed by SDS-PAGE and in-gel fluorescence analysis (Fig. S2b). Flow cytometry further demonstrated that the two-step click reaction did not impair the binding affinity of αAPN-VHH-AzF to APN (Fig. S2c). Based on these promising results, we proceeded to apply the same conjugation strategy to TCO-LNPs. This allowed for successful VHH conjugation without inducing LNP aggregation (Fig. 2b), thus enabling stable and functional nanoparticle formulations for targeted delivery. To optimize the conjugation efficiency of VHH-AzF with TCO-LNPs, we tested two strategies (Fig. 2c). In Strategy 1 (S1), VHH-AzF was first conjugated with DBCO-Tz via a SPAAC reaction to form VHH-Tz, followed by an IEDDA reaction with TCO-LNPs. However, Coomassie staining revealed the presence of free VHH-AzF at different molar ratios (Fig. 2d). In a second strategy (S2), TCO-LNPs were first reacted with DBCO-Tz via an IEDDA reaction, and the generated DBCO-LNPs were then conjugated with VHH-AzF using a SPAAC reaction. This significantly reduced (ctrl-VHH, 1:10) or completely eliminated (αAPN-VHH) the amount of free VHH-AzF (Fig. 2d).

We then optimized the molar ratio of TCO-LNP: DBCO-tetrazine: VHH-AzF (Fig. S3). Using a 10-fold excess of VHH-AzF (1:1:10) led to poor labeling and binding of the VHH-LNPs to BHK-APN cells, likely due to free VHH competition. Reducing the amount of VHH-AzF (1:1:2) improved binding of the LNPs, while increasing DBCO-tetrazine (1:5:2) yielded the highest APN-specific fluorescence. Further increasing the amount of the linker (1:10:2) showed no added benefit.

Next, we characterized the biophysical properties of the VHH-functionalized LNPs using dynamic light scattering (Fig. 2e-h; Table 1). LNP size increased across conjugation steps, from TCO-LNPs (172.02  $\pm$  10.38 nm) to  $\alpha$ APN-VHH-LNPs (231.29  $\pm$  17.38 nm) and Ctrl-VHH-LNPs (269.69  $\pm$  8.37 nm), indicating successful surface modification (Fig. 2e-f). In contrast, the polydispersity index and zeta potential remained relatively stable across all LNP formats (Fig. 2g-h; Table 1), suggesting that VHH conjugation did not alter these parameters. We next sought to determine whether the APN-specific single

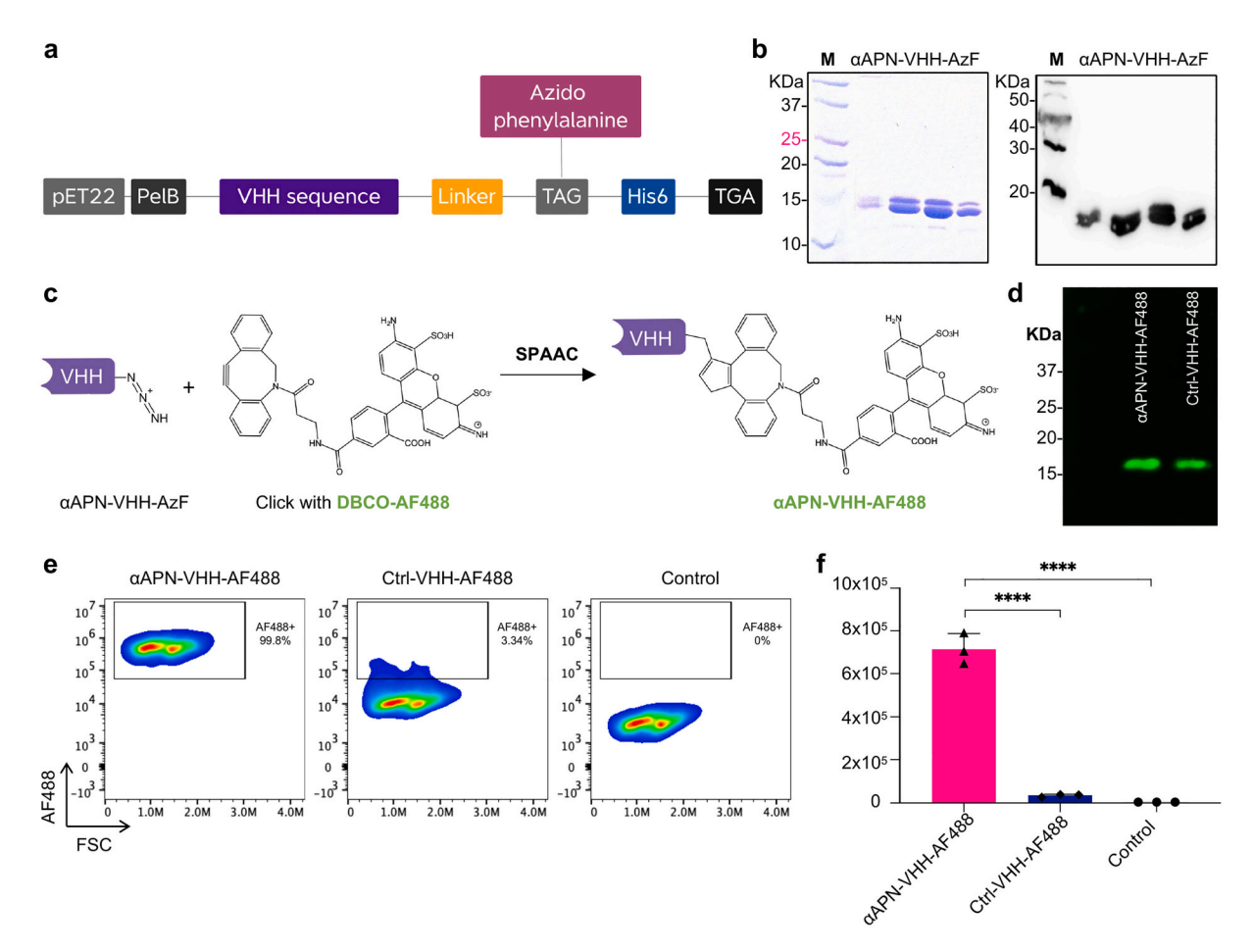


Fig. 1. Production of para-Azido phenylalanine-modified anti-APN single-domain antibodies. a) Design of APN-specific VHH containing integrated azido-phenylalanine ( $\alpha$ APN-VHH-AzF). b) Coomassie staining (left) and VHH-specific western blot (right) showing purified  $\alpha$ APN-VHH-AzF from different batches (10 μL loaded per sample). c) Schematic of the strain-promoted azido-alkyne cycloaddition (SPAAC) reaction between azido-functionalized VHH (VHH-AzF) and DBCO-AF488, resulting in the formation of VHH-AF488 through a one-step conjugation strategy. d) Fluorescent SDS-PAGE (AF488 channel) confirms successful labelling of VHH with AF488. A total of 1 μg of VHH-AF488 was loaded per lane. e) Representative flow cytometry plots showing the binding of  $\alpha$ -APN-AF488 and Ctrl-VHH-AF488 to BHK-APN cells after 1 h incubation at 4 °C. Conjugates were prepared using either one-step or two-step click chemistry. f) Quantitative flow cytometry analysis of APN binding. Data represent mean  $\pm$  SD from independent batches (n = 3) of  $\alpha$ APN-VHH-AzF. Data were analyzed by one-way ANOVA. \*\*\*\*, p < 0.0001. M: molecular weight marker.

domains antibodies decorating the surface of the LNPs could still bind their target. Taking advantage of the particulate form of the LNPs, an ELISA was designed to confirm the presence of VHHs on the LNPs (Fig. 2i). The results showed the ability of the APN-specific VHHs grafted on the LNP surface to bind their target (Fig. 2j).

# 3.2. APN-targeted VHH-LNPs deliver mRNA to cells

We have previously shown that targeting proteins and yeast microparticles to APN on intestinal epithelial cells leads to their internalization by these cells [30,31,33]. To understand whether LNPs are also taken up by APN-expressing cells when targeted to APN, LNPs were labeled with Cy5 by substituting 0.1 % of DSPC with DSPC-Cy5 for tracking purposes (Fig. 3a). Flow cytometry revealed that  $\alpha$ APN-VHH-LNPs bound to BHK-APN cells (Fig. 3b). To further assess the specificity of this binding,  $\alpha$ APN-VHH-LNPs were incubated with both APN-expressing BHK-APN cells and control BHK cells. Flow cytometry data showed that BHK-APN cells exhibited significantly higher nanoparticle binding as compared to BHK cells (Fig. 3c). In addition, confocal microscopy showed that the APN-targeted VHH-LNPs were taken up by BHK-APN cells in contrast to BHK cells (Fig. 3d). To investigate how TCO content affected LNP uptake, we varied the ratio of DSPE-PEG\_2000-TCO and DMG-PEG\_2000 while maintaining a total PEG-lipid content of 1.5

mol%. As shown in **Fig. S4a-c**, decreasing the proportion of TCO-PEG $_{2000}$ -DSPE reduced  $\alpha$ APN-VHH-LNP internalization. This reduction is most likely due to the lower number of TCO groups available for VHH conjugation. Together, these findings illustrate that the  $\alpha$ APN-VHH-LNPs effectively bind to and are taken up by APN-expressing cells in an APN-dependent manner.

Next, we wanted to investigate the potential of the  $\alpha$ APN-VHH-LNPs as carriers for mRNA delivery. The different Cy5-labeled LNP formats were loaded with mRNA encoding eGFP at an efficiency of 77.57 %  $\pm$ 2.14 % (Fig. 4a). These Cy5-labeled mRNA-loaded LNPs (DBCO-LNP, ctrl-VHH-LNP, and αAPN-VHH-LNP) were not cytotoxic to BHK-APN cells at concentrations up to 5 µL LNP in 100 µL medium (Fig. S5a). Subsequently, the Cy5-labeled mRNA-loaded LNPs were added to BHK-APN cells at varying amounts. Upon incubation, APN-targeted mRNAloaded LNPs resulted in a significant concentration-dependent increase in the Cy5 and GFP signal of the BHK-APN cells as compared to the control conditions. This indicates that targeting the LNPs to APN results in an enhanced uptake and subsequent translation of the eGFP mRNA (Fig. 4b-d). We also found that the control LNPs were taken up by the BHK-APN cells. To understand how the Cy5 intensity is linked to GFP expression, we further categorized the cells into Cy5+ (intensity  $>10^5$ ) and Cy5dim (intensity  $10^3$ – $10^5$ ) populations (Fig. 4b, S5c). This revealed that most cells in the control groups resided within the Cy5dim

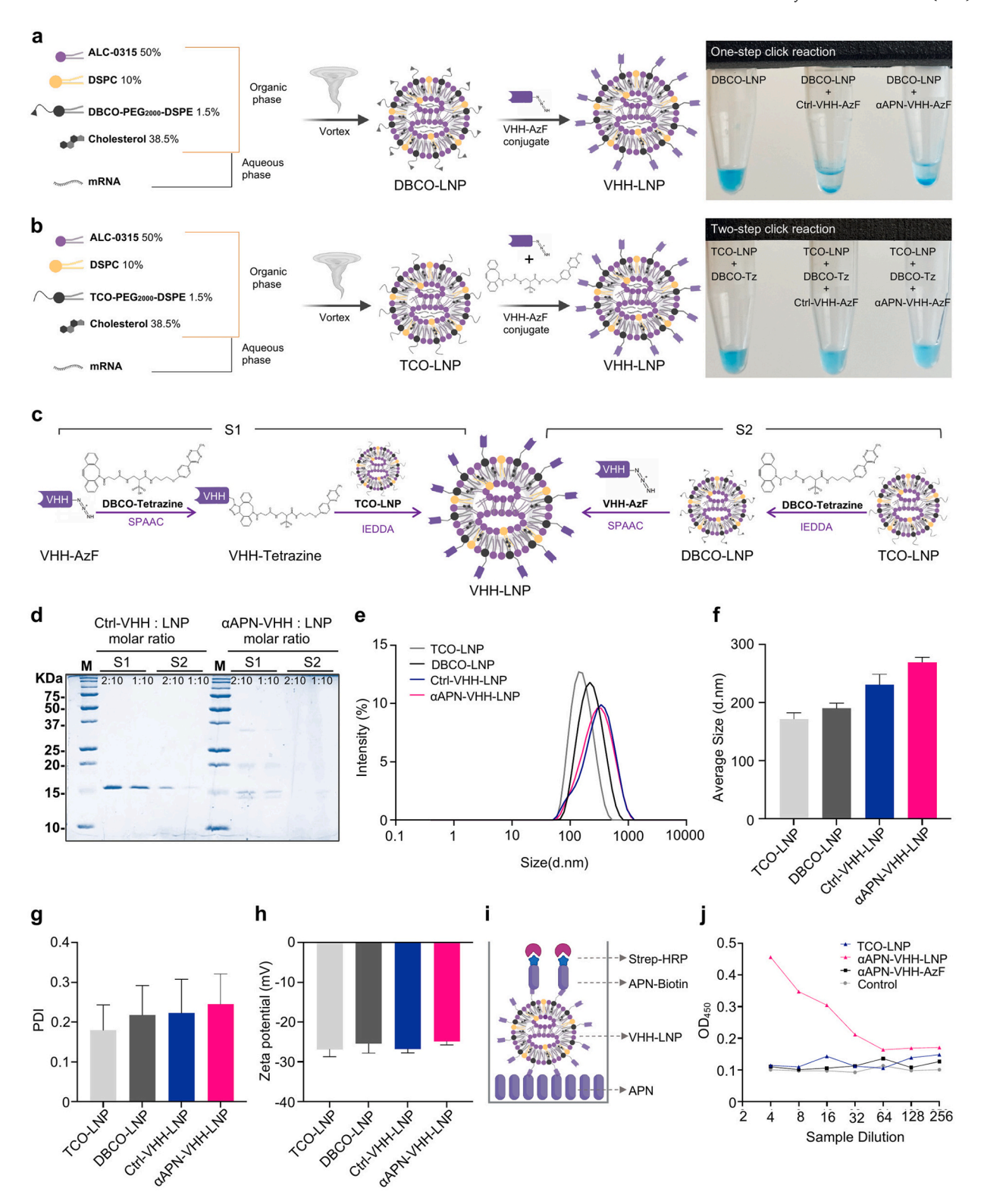


Fig. 2. Characterization of VHH-Functionalized Lipid Nanoparticles. a, b) Schematic representations of  $\alpha$ -APN-LNP synthesis via a) one-step and b) two-step click reactions. Representative images of Cy5-labeled LNPs from each method are shown to the right. LNPs were formulated with ALC-0315 (50 %), DSPC (10 %), cholesterol (38.5 %), DBCO-PEG<sub>2000</sub>-DSPE (1.5 %), or TCO-PEG<sub>2000</sub>-DSPE (1.5 %) by mixing an organic and aqueous phase containing mRNA, followed by vortexing. The VHH-AzF ligand was then conjugated to the pre-formed LNPs directly a) or via a soluble DBCO-tetrazine intermediate b) to generate αAPN-VHH-LNP or Ctrl-VHH-LNP. c) Graphical representation of the two conjugation strategies: Strategy 1 (S1) and Strategy 2 (S2) for attaching VHH-AzF to the LNP surface. d) SDS-PAGE (10 %) analysis of VHH-LNPs (10 μL) reveals unclicked single domain antibodies for both strategies at different molar ratios, visualized by Coomassie staining. e-h) Physical properties of TCO-LNPs, DBCO-LNPs, Ctrl-VHH-LNPs, and αAPN-VHH-LNPs were characterized via dynamic light scattering (DLS). e) Size distribution; f) Average size (diameter, nm); g) Polydispersity index (PDI); h) Zeta potential (mV). Data represent the mean ± SD from n = 10 independent batches. i, j) The presence of APN-specific VHH on the LNP surface was determined using ELISA. i) Schematic of the ELISA setup: APN-coated plates were incubated with αAPN-VHH-LNPs, and VHHs were detected using biotinylated APN (APN-Biotin) and streptavidin-HRP (Strep-HRP). j) Absorbance at 450 nm, with the X-axis indicating sample dilution.

**Table 1** Average particle size, polydispersity index (PDI), and zeta potential of the different LNP formulations. Data represent mean  $\pm$  standard deviation (SD) from independent batches (n=10). Measurements were performed in 5 mM HEPES buffer (pH 7.4) using dynamic light scattering (DLS) for size and PDI, and electrophoretic light scattering for zeta potential.

electrophoretic right scattering for zeta potential.				
	TCO-LNP	DBCO-LNP	Ctrl-VHH- LNP	α-APN-VHH- LNP
Particle size (d.nm) Polydispersity Index	$172.02 \pm \\ 10.38 \\ 0.18 \pm 0.06$	$194.23 \pm \\ 4.59 \\ 0.20 \pm 0.11$	$\begin{array}{c} 269.69 \pm \\ 8.37 \\ 0.25 \pm 0.08 \end{array}$	$\begin{array}{c} 231.29 \pm \\ 17.38 \\ 0.22 \pm 0.09 \end{array}$
Zeta potential	$-26.87\ \pm$	$-31.30\ \pm$	$-24.87\ \pm$	$-26.77\ \pm$
(mV)	1.82	3.22	0.88	1.00

population, while over half of the cells treated with  $\alpha APN-VHH-LNP$  were in the Cy5+ population. Interestingly, upon analyzing GFP expression in these cell populations, it was found that over 80 % of GFP-positive cells in the  $\alpha APN-VHH-LNP$  group were in the Cy5+ population, whereas GFP-positive cells in the control groups were predominantly in the Cy5dim population (Fig. S5c). This suggests that APN-mediated targeting significantly enhances the uptake of LNPs, leading to increased mRNA translation. Aligning with these flow cytometry results, confocal microscopy revealed a substantial increase in uptake and GFP expression of the  $\alpha APN-VHH-LNPs$  as compared to the control conditions (Fig. 4e).

To further differentiate APN receptor-mediated binding from nonspecific interactions, we reduced the incubation temperature to inhibit energy-dependent processes, such as endocytosis, thereby minimizing nonspecific uptake [39]. The results demonstrated that lowering the temperature significantly reduced nanoparticle binding in the

control groups, whereas  $\alpha APN\text{-}VHH\text{-}LNPs$  retained strong binding (Fig. S5d). After minimizing nonspecific interactions, only BHK-APN cells treated with  $\alpha APN\text{-}VHH\text{-}LNPs$  expressed GFP, confirming that APN-mediated binding is essential for efficient nanoparticle uptake and mRNA translation. These findings collectively illustrate that  $\alpha APN\text{-}VHH\text{-}LNPs$  efficiently target APN, enhancing LNP internalization and promoting successful delivery and subsequent translation of the encapsulated mRNA.

Building further on these results, we explored the potential of αAPN-VHH-LNPs for delivering mRNA to porcine intestinal epithelial cells. Similar to BHK-APN cells, the various LNP formulations were not cytotoxic to APN-expressing porcine intestinal epithelial cells (IPEC-J2-APN) (Fig. S5b). Moreover, APN targeting by VHH-LNPs led to increased uptake of LNPs and elevated GFP expression in these cells as compared to control LNPs, as shown by flow cytometry and confocal microscopy (Fig. 4f-h). Interestingly, we observed lower overall uptake and expression levels in IPEC-J2-APN cells than in BHK-APN cells, likely due to the lower APN expression in the former (Fig. S5e). Alternatively, endosomal maturation and trafficking pathways might differ between the two cell types. Since the maturation of endosomes coincides with their acidification, VHHs were labeled with the pH-sensitive fluorochrome pHrodo to assess differences in endosomal acidification. In BHK-APN cells, APN-mediated uptake of LNPs triggered endosomal acidification at 4 h, which further increased at 24 h (Fig. S6a,b). In IPEC-J2-APN cells, however, the endosomal pH did not increase at 4 h, with a modest increase at 24 h (Fig. S6c,d). This difference in endosomal acidification between the two cell types corresponded with the differences in Cy5 and GFP expression at later time points. In BHK-APN cells, Cy5 MFI values declined from 24 to 48 h, likely reflecting the clearance of Cy5-labeled lipids upon LNP degradation, while GFP levels increased,

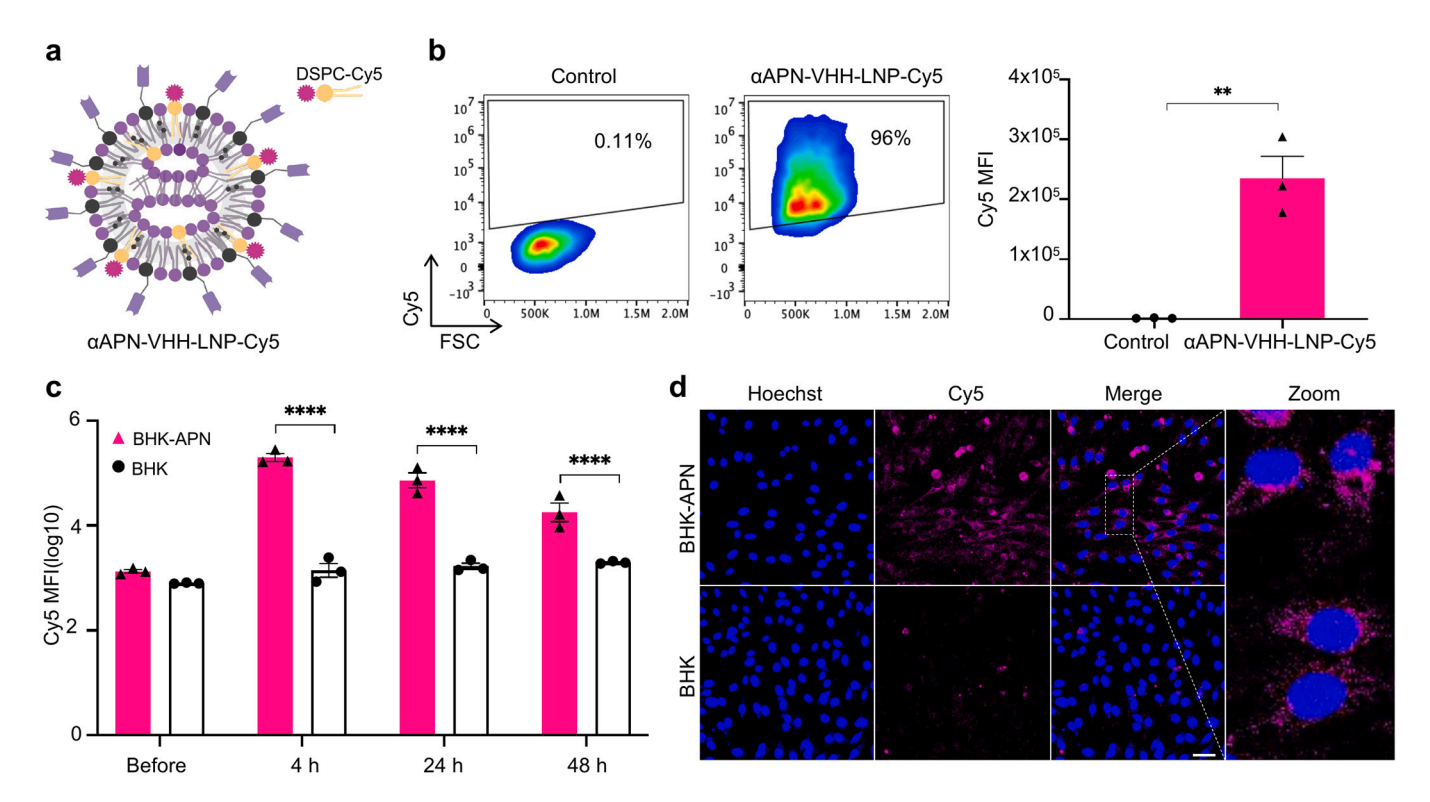
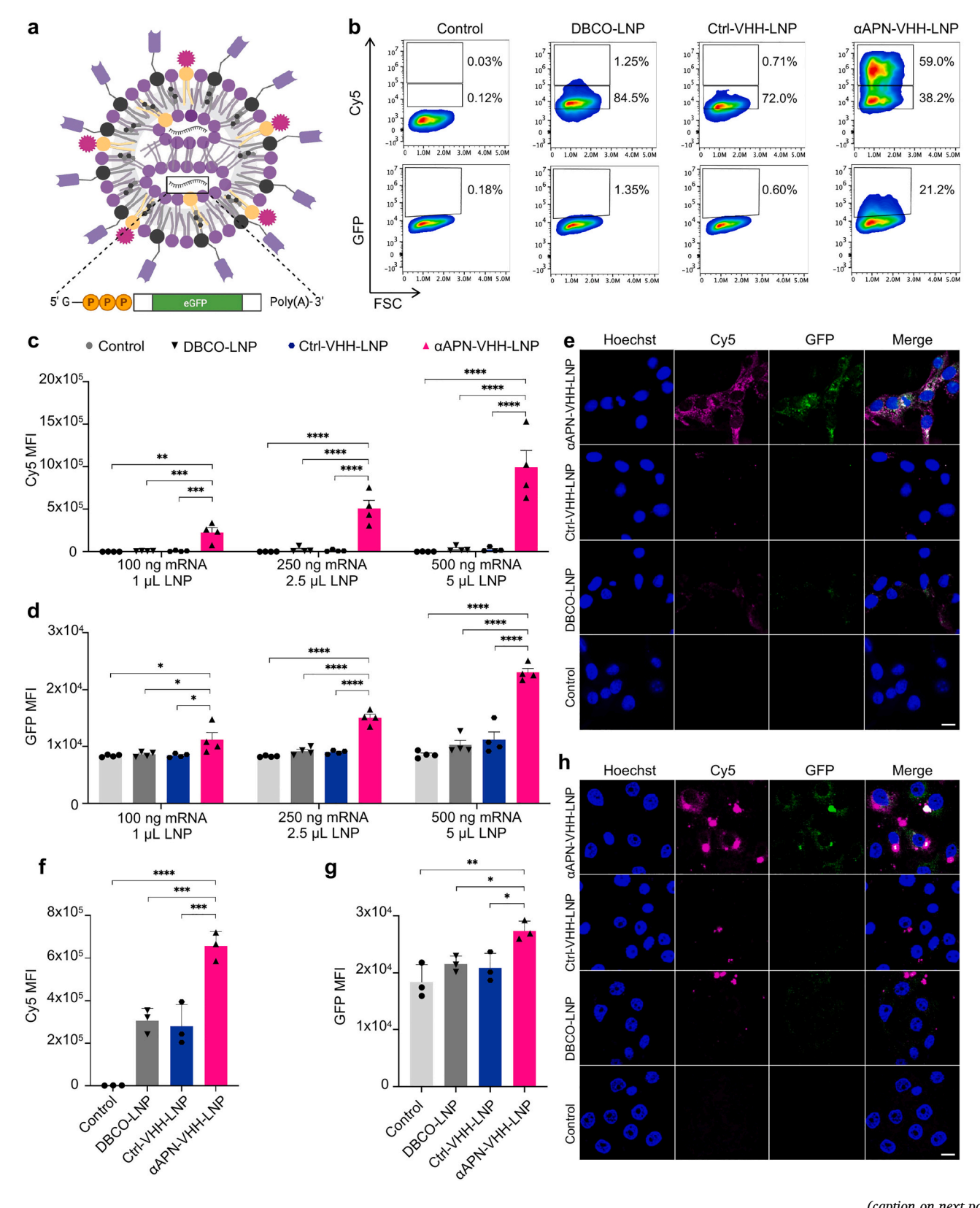


**Fig. 3.** Binding and Uptake of APN-Targeted VHH-LNPs by an APN-Expressing Cell Line. a) Schematic illustration of Cy5-labeled αAPN-VHH-LNPs. b) Representative flow cytometry plots and percentages depicting the binding of Cy5-labeled αAPN-VHH-LNPs to BHK-APN cells, with untreated BHK-APN cells as a control. Data represent mean  $\pm$  SD from n=3 independent experiments. Data were analyzed using an unpaired t-test. \*\*, p < 0.01. c) Flow cytometry analysis of Cy5-labeled αAPN-VHH-LNP binding to BHK-APN and BHK cells following 1 h of incubation at 4 °C. Non-bound LNPs were washed off, and cells were incubated at 37 °C for various time points (4 h, 24 h, 48 h). Data represent mean  $\pm$  SD from n=3 independent experiments. Data were analyzed using multiple unpaired t-tests. \*\*\*\*, p < 0.0001. d) Confocal microscopy images showing the internalization of Cy5-labeled αAPN-VHH-LNPs by BHK-APN cells after 24 h of incubation. Images are representative of 3 independent experiments. Scale bar: 50 μm. MFI: mean fluorescence intensity.



(caption on next page)

Fig. 4. APN-Mediated mRNA Delivery to APN-Expressing Cells Using APN-Targeted VHH-LNPs. a) Schematic illustration of Cy5-labeled αAPN-VHH-LNPs encapsulating eGFP mRNA with EE% (encapsulation efficiency) = 77.57 %  $\pm$  2.14 %. b) Representative flow cytometry plots and percentages depicting VHH-LNP (5 μL, 500 ng mRNA) internalization and GFP expression by BHK-APN cells after 24 h incubation at 37 °C. c,d) Flow cytometry analysis showing internalization (Cy5 MFI) and mRNA translation (GFP MFI) in BHK-APN cells. Data are presented as mean  $\pm$  SD from n=4 independent experiments. Data analyzed by one-way ANOVA.\*\*, p < 0.001; \*\*\*\*, p < 0.0001; \*\*\*\*, p < 0.0001. e) Confocal microscopy images showing the internalization of VHH-LNPs (7.5 μL, 750 ng mRNA per 24-well) and GFP expression in BHK-APN cells after 24 h incubation at 37 °C. Nuclei were stained with Hoechst (blue), LNPs were labeled with Cy5 (magenta), and GFP expression is shown in green. Colocalization of Cy5 and GFP signals appears white in the merged images. Images are representative of 4 independent experiments. f,g) Flow cytometry evaluation of VHH-LNP internalization (Cy5 MFI) and mRNA translation (GFP MFI) in porcine small intestinal epithelial cells (IPEC-J2-APN). Data represent mean  $\pm$  SD from n = 3 independent experiments. Data analyzed by one-way ANOVA. \*, p < 0.05; \*\*, p < 0.01; \*\*\*\*, p < 0.001; \*\*\*\*, p < 0.0001. h) Confocal microscopy images showing VHH-LNP internalization (7.5 μL, 750 ng mRNA per 24-well) and GFP expression in IPEC-J2-APN cells after 24 h incubation at 37 °C. Nuclei were stained with Hoechst (blue), LNPs were labeled with Cy5 (magenta), and GFP expression is shown in green. Colocalization of Cy5 and GFP signals appears white in the merged images. Images are representative of 3 independent experiments. Scale bar = 25 μm. MFI: mean fluorescence intensity. (For interpretation of the references to colour in this figure legend, the reader is referred to the web version of this article.)

indicating efficient endosomal escape and mRNA release for GFP translation (Fig. S6e). Conversely, in IPEC-J2-APN cells, Cy5 MFI values increased over the same period without an increase in GFP MFI values (Fig. S6f). These results are consistent with the endosomal trafficking dynamics in polarized epithelial cells, which often sort internalized molecules toward recycling or transcytotic pathways. Such routing might limit the exposure of LNPs to acidic conditions needed for endosomal escape, thereby restricting mRNA release and the relatively low GFP expression levels in IPEC-J2-APN cells.

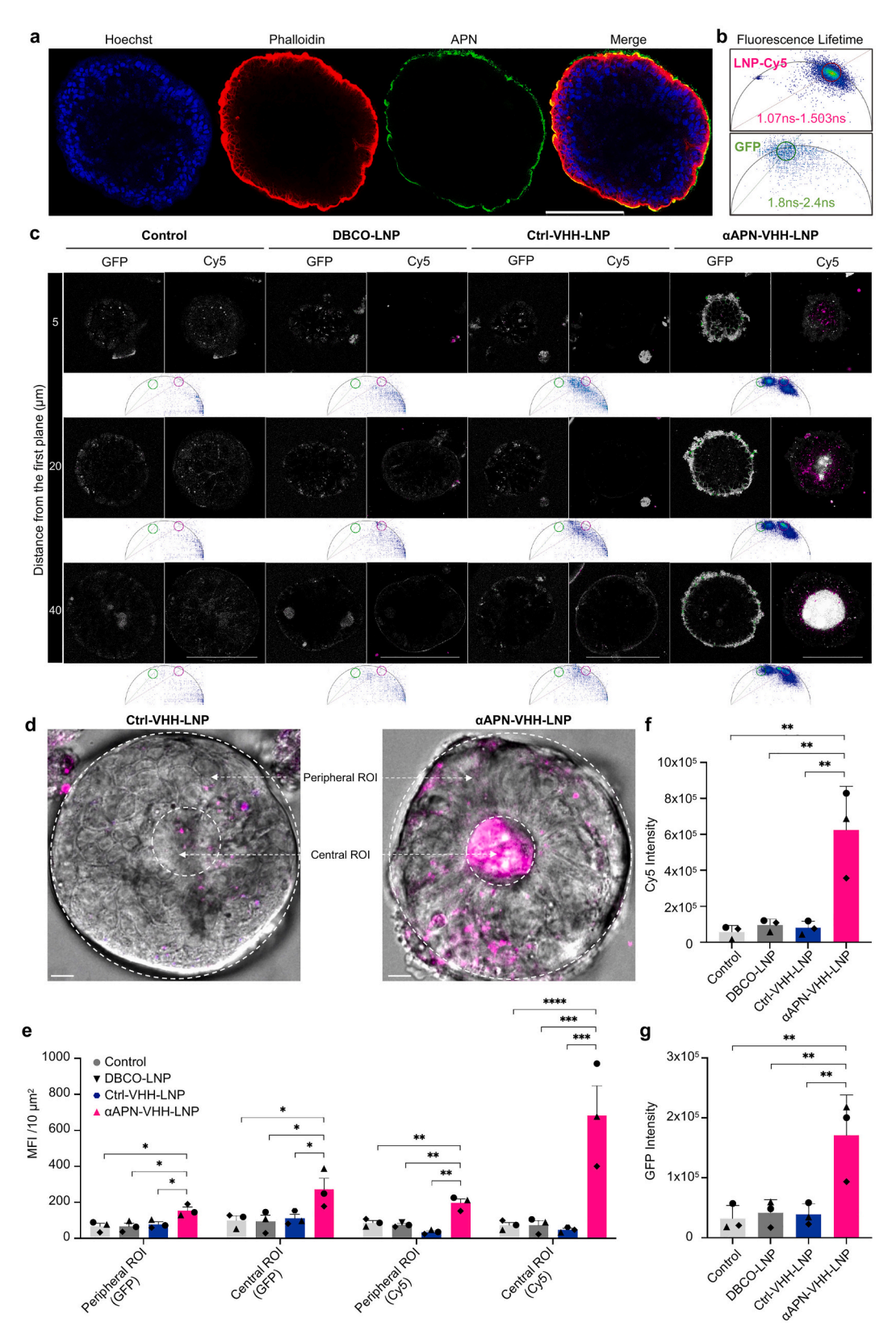
# 3.3. APN-mediated transport of mRNA-LNPs across the small intestinal epithelium

Previous experiments confirmed the potential of αAPN-VHH-LNP to deliver LNPs to intestinal epithelial cells. To further explore its applicability in a model that better represents the in vivo small intestinal epithelium, we used porcine small intestinal organoids (enteroids). Enteroids cultured in basal membrane extracts, like Matrigel or Cultrex, typically adopt a basal-out topology [40]. In these basal-out enteroids, the apical membrane faces the pseudolumen, making it challenging to study the interaction of LNPs with the apical side of the gut epithelium. To facilitate this, we used either monolayers derived from these enteroids or apical-out enteroids. When basal-out enteroids are cultured without BME, they spontaneously revert their topology from basal-out to apical-out [36]. Of note, APN is expressed by primary intestinal epithelial cells when cultured as monolayers (Fig. S7a) or as apical-out enteroids (Fig. 5a). In enteroid monolayers, APN targeting resulted in an increased uptake of the LNPs as compared to the controls, as evidenced by confocal microscopy (Fig. S7b). This VHH-LNP uptake correlated with GFP expression, which co-localized with the Cy5 signal. These results indicate that APN-targeted LNPs are internalized by primary intestinal epithelial cells. Targeting of antibody-antigen fusion proteins or microparticles to APN results in their transcytosis across the gut epithelial layer [31-33]. To understand whether APN-targeted mRNA-LNPs are also transported through the intestinal epithelium, we used apical-out enteroids, 3D confocal microscopy and Fluorescence Lifetime Imaging Microscopy (FLIM). This approach allows for the distinction of LNP and GFP signals from autofluorescence, which was noticed in the intestinal organoid model [41]. For the FLIM analysis, we first measured the 'fingerprint' fluorescence lifetime (τ) of freshly made Cy5-labeled VHH-mRNA-LNPs in PBS as well as GFP in BHK-APN cells, where GFP expression (after incubation with αAPN-VHH-LNP for 24 h) was confirmed by flow cytometry. As shown in the phasor plots, Cy5-labeled VHH-mRNA-LNPs had a  $\tau$  =1.17–1.50 ns and GFP a  $\tau$  =1.80–2.40 ns (Fig. 5b). After incubating apical-out enteroids for 48 h with Cy5-labeled APN-targeted mRNA-LNPs, 3D confocal microscopy confirmed the presence of both Cy5 and GFP signals within the enteroids as compared to the controls (Fig. 5c,d). When evaluating the Cy5 fluorescence lifetime of the LNPs internalized by the enteroids, a broader range of Cy5 lifetimes was observed on the phasor plots as compared to the fingerprint. This shift in fluorescence lifetime can be attributed to different micro-environments, such as changes in pH [42,43]. We then selected

the Cy5 fluorescent lifetime events corresponding to this Cy5 fingerprint and pseudocolored these purple on the confocal images. These purplecolored VHH-mRNA-LNPs most likely reflect LNPs that are being transcytosed through the intestinal epithelial cells. In contrast, Cy5 signals with a shifted lifetime were pseudocolored white on the confocal images. The vast majority of these Cy5-labeled VHH-mRNA-LNPs accumulated in the center of the apical-out enteroids, while a minority resided in vesicles with a different microenvironment than vesicles containing the purple-colored LNPs. These observations suggest that targeting of the LNPs to APN resulted in their intact transport across the intestinal epithelial cells and their release in the center of the enteroids. To further understand the fate of the APN-targeted mRNA-LNPs, we evaluated Cy5 and GFP fluorescence intensity in regions of interest (ROIs) corresponding to the epithelial layer (peripheral ROI) and the subepithelial compartment (central ROI) (Fig. 5d). APN targeting resulted in increased Cy5 levels in the peripheral and central ROI than in the control groups (Fig. 5e). Moreover, fluorescence intensity measurements supported this finding (Fig. 5f,g), showing significantly higher Cy5 and GFP levels in the APN-targeted groups. These observations underscore the enhanced delivery and expression achieved by APN-targeted LNPs. Together, our findings show that the majority of the APN-targeted mRNA-LNPs are transported through the gut epithelial cells and subsequently accumulate into the center of the enteroids.

# 3.4. APN-targeted LNPs facilitate in vivo uptake and delivery to mesenteric lymph nodes

To assess the uptake of APN-targeted VHH-mRNA-LNPs by the small intestinal tissues in vivo, we performed a gut-ligated loop model in piglets. Due to potential oral and organ toxicity associated with DSPC-Cy5, we formulated DiD-labeled TCO-LNPs by substituting 0.1 mol% of DSPC-Cy5 with DiD. Physicochemical characterization confirmed that DiD-labeled TCO-LNPs retained a comparable size, PDI, and zeta potential as their Cy5-labeled counterparts (Fig. S8a, Table 1). Cell viability assays in BHK-APN cells showed no cytotoxicity after 24 h incubation with DiD-labeled LNPs (Fig. S8b). Moreover, DiD-labeled αAPN-VHH-LNPs maintained efficient cellular uptake and GFP expression in vitro (Fig. S8c-e). For the in vivo experiment, DiD-labeled mRNA-LNPs were administered directly into the lumen of the gut ligated loops and incubated for 6 h, followed by analysis of their distribution in the intestinal tissue by confocal microscopy. As compared to the controls, APN-targeted VHH-mRNA-LNPs were taken up by villus epithelial cells and by cells underneath the gut epithelium, most likely antigenpresenting cells. Both in the gut epithelial cells and the underlying cells, APN-targeting of the mRNA-LNPs resulted in delivery of mRNA and the subsequent translation into GFP (Fig. 6a,c,d). In addition, APN targeting also resulted in the uptake of mRNA-LPNs by gut epithelial cells and underlying cells in the crypt regions, while this was completely absent in the controls (Fig. S9). To assess whether this uptake of the APN-targeted mRNA-LNPs also resulted in their presence in mesenteric lymph nodes, we collected the lymph nodes that drained the gut loops and performed confocal microscopy on tissue sections. Interestingly,



(caption on next page)

Fig. 5. APN-mediated mRNA delivery to porcine enteroids. a) Confocal images of apical-out enteroids stained for APN (green) and F-actin (Phalloidin, red), with nuclei counterstained using Hoechst (blue). Scale bar = 100 μm. b) Phasor plots representing the 'fingerprint' fluorescence lifetime measurement of VHH-LNP-Cy5 (LNP-Cy5) and GFP. c) *Z*-stack with corresponding phasor plots and fluorescent images of apical-out enteroids incubated with different LNP formulations, evaluated via FLIM. GFP channel: Pseudocolored green indicates GFP lifetimes matching the lifetime of GFP in BHK-APN cells (1.80–2.40 ns); white indicates shifted GFP lifetimes within the enteroid microenvironment. Cy5 channel: Pseudocolored purple represents Cy5-labeled VHH-LNPs with fluorescence lifetimes consistent in PBS (1.07–1.50 ns); white indicates Cy5 lifetime shifted with the enteroid micro-environment. Scale bar = 100 μm. d) 3D Confocal images merged with transmission light and Cy5 channels (LNPs: purple), showing the selection of regions of interest (ROIs) in enteroids incubated for 48 h with 7.5 μL of Ctrl-VHH-LNPs (left) and αAPN-VHH-LNPs (right) at 37 °C. ROIs are defined as the central ROI and peripheral ROI (white dashed lines). Scale bar = 10 μm. e) Comparative analysis of GFP or Cy5 mean fluorescence intensities (per 10 μm²) between central and peripheral ROIs after 48 h of incubation at 37 °C. The experiment was performed with 3 biological replicates (organoids from  $\blacksquare$  Pig 1,  $\blacksquare$  Pig 2,  $\blacksquare$  Pig 3), selecting 5–7 enteroids per condition. Data quantified based on maximum intensity projection (MIP) z-stack images of selected organoids. Data analyzed by one-way ANOVA. \*\*P < 0.05; \*\*, p < 0.01; \*\*\*, p < 0.001; \*\*\*\*, p < 0.001. f,g) Comparative analysis of Cy5 and GFP intensities across different experimental groups after 48 h incubation at 37 °C. The experiments were conducted with 3 biological replicates (organoids from  $\blacksquare$  Pig 1,  $\blacksquare$  Pig 3), selecting 5–7 apical-out organoids per condition. Data quantified based on maximum in

both DiD and GFP fluorescence intensity were higher in lymph nodes draining the gut loops incubated with APN-targeted VHH-LNPs as compared to those draining the control loops (Fig. 6b,e,f). Together, these *in vivo* findings align well with our in vitro data and support the conclusion that APN-targeted mRNA LNPs enable the delivery of mRNA to the small intestinal epithelium.

and underlying cells as well as to the presence of DiD and GFP to the local draining lymph nodes, where immune responses are initiated.

#### 4. Discussion

Here, we report on the development of a programmable LNP platform that enables cell type-specific delivery of mRNA payloads by surface decorating the LNPs with single domain antibodies or VHHs via click chemistry. By leveraging our expertise and tools in APN targeting [30–33], we demonstrate the potential of this platform to facilitate the delivery of mRNA to the gut tissues since mRNA-loaded LNPs targeted to aminopeptidase N are transported across the small intestinal epithelium in apical-out enteroids and under in vivo conditions. These findings support future research on cell-type-specific mRNA-based therapeutics.

A limitation of current mRNA-LNP therapeutics is their accumulation in the liver. Several methods have been investigated to deliver mRNA-LNPs to specific tissues or cells, such as by changing the lipid composition (SORT-LNPs) [20] or by conjugating affinity ligands, like antibodies [44]. Here, we used single domain antibodies (VHHs) since these offer unique advantages as compared to conventional antibodies. VHHs (15 kDa) are smaller than conventional antibodies (150 kDa), have greater stability in a variety of conditions, and lack an Fc region, which reduces the activation of immune cells, decreasing the risk of adverse reactions and making them suitable for repeated administrations [45]. Due to their small size, their conjugation might also have less impact on the physical properties of the LNPs than conventional antibodies. The size of the LNPs plays an important role in their intracellular fate. LNPs <200 nm are generally more suitable for endosomal escape and cytoplasmic release, while larger particles are directed toward lysosomal degradation pathways [46-48]. Functionalizing the LNPs with VHHs resulted in LNPs with similar physical properties, although an increase in the average size was observed. While this might affect their intracellular fate, microfluidic mixing or membrane filtration could allow to better control the size distribution of the VHH-LNPs [49].

To achieve site-specific functionalization of LNPs with VHHs, we incorporated the non-canonical amino acid para-azido-phenylalanine (AzF) at the C-terminus of both  $\alpha$ APN-specific and control VHHs using an engineered *E. coli* expression system. This genetic strategy circumvents the need for post-translational chemical modifications with hydrophobic linkers such as TFP-PEG(4)-DBCO, commonly used in previous studies [23,50,51]. In contrast, our VHH-AzF constructs were produced at a high yield, remained soluble in aqueous buffer, and retained their reactivity even after long-term storage at  $-20~^{\circ}\text{C}$  without stabilizers like glycerol [52].

Functionalisation of DBCO-LNPs with VHH-AzF using a one-step SPAAC click reaction resulted in severe LNP aggregation and a complete loss of APN binding and mRNA delivery. These results match prior reports showing that LNPs modified with DSPE-PEG  $_{2000}\text{-}DBCO$  (0.1 %--0.3 % molar ratio) and then reacted with azide groups cause a twofold increase in particle size and PDI, and lead to the formation of micellar aggregates and multilamellar structures, disrupting the spherical morphology of the LNPs [53]. These findings indicate the limitations of DBCO-mediated SPAAC for direct surface functionalization of LNPs. Using a sequential SPAAC-IEDDA approach with TCO-modified LNPs and a water-soluble DBCO-tetrazine (DBCO-Tz) linker avoided LNP aggregation and preserved mRNA delivery to cells. Notably, the sequence of the click reaction steps was crucial. TCO-LNPs needed to be modified first with DBCO-Tz and then conjugated with VHH-AzF, because the reversed sequence resulted in a high amount of unbound VHH-AzF, likely due to residual DBCO-Tz competing with VHH-Tz in the IEDDA reaction. Our results are supported by recent studies showing that DBCO-labeled antibodies tend to aggregate when conjugated to liposome-Azido via a SPAAC reaction, while an alternative click chemistry reaction using TCO-tetrazine showed minimal antibody aggregation. This difference is likely attributable to the lower hydrophobicity of TCO (estimated to be 3.8-fold less than DBCO) [54], making TCOtetrazine conjugation a more stable and biocompatible option for surface functionalization. While the current workflow results in reproducible VHH-conjugated LNPs, future improvements may simplify this process. For example, incorporating tetrazine-functionalized amino acids into the VHHs would allow a one-step IEDDA click reaction with TCO-LNPs [55].

Functionalization of mRNA-loaded LNPs with APN-specific VHHs enabled their uptake by APN-expressing cells, which resulted in the translation of the encapsulated mRNA to GFP. However, we noticed differences in GFP expression levels between the two APN-expressing cell lines. In the BHK-APN cell line (fibroblasts), internalization of the APN-targeted mRNA-LNPs resulted in high GFP expression levels, while in the IPEC-J2-APN cell line (intestinal epithelial cells), uptake of the APN-targeted mRNA-LNPs resulted in low GFP expression levels. These differences might be attributed to the different endosomal maturation and trafficking pathways in epithelial cells and fibroblasts upon APNmediated uptake. In BHK-APN cells, internalization of the LNPs resulted in endosomal acidification, as shown by increased pHrodo fluorescence. This drop in pH is necessary for ionizable lipids, such as ALC-0315, to rupture the endosomal membrane and release mRNA payloads into the cytoplasm. In contrast, in IPEC-J2-APN cells, uptake of LNPs steadily increased, but this resulted in limited endosomal acidification and, thus, low GFP expression levels. This suggests that in epithelial cells, the LNPs are routed to pathways that limit cytoplasmic release. This aligns not only with other reports, which showed that in gut epithelial cells, vesicle sorting mechanisms often route endosomes to recycling or transcytosis pathways, thereby avoiding endosomal acidification, but also with our previous studies on APN-mediated transport

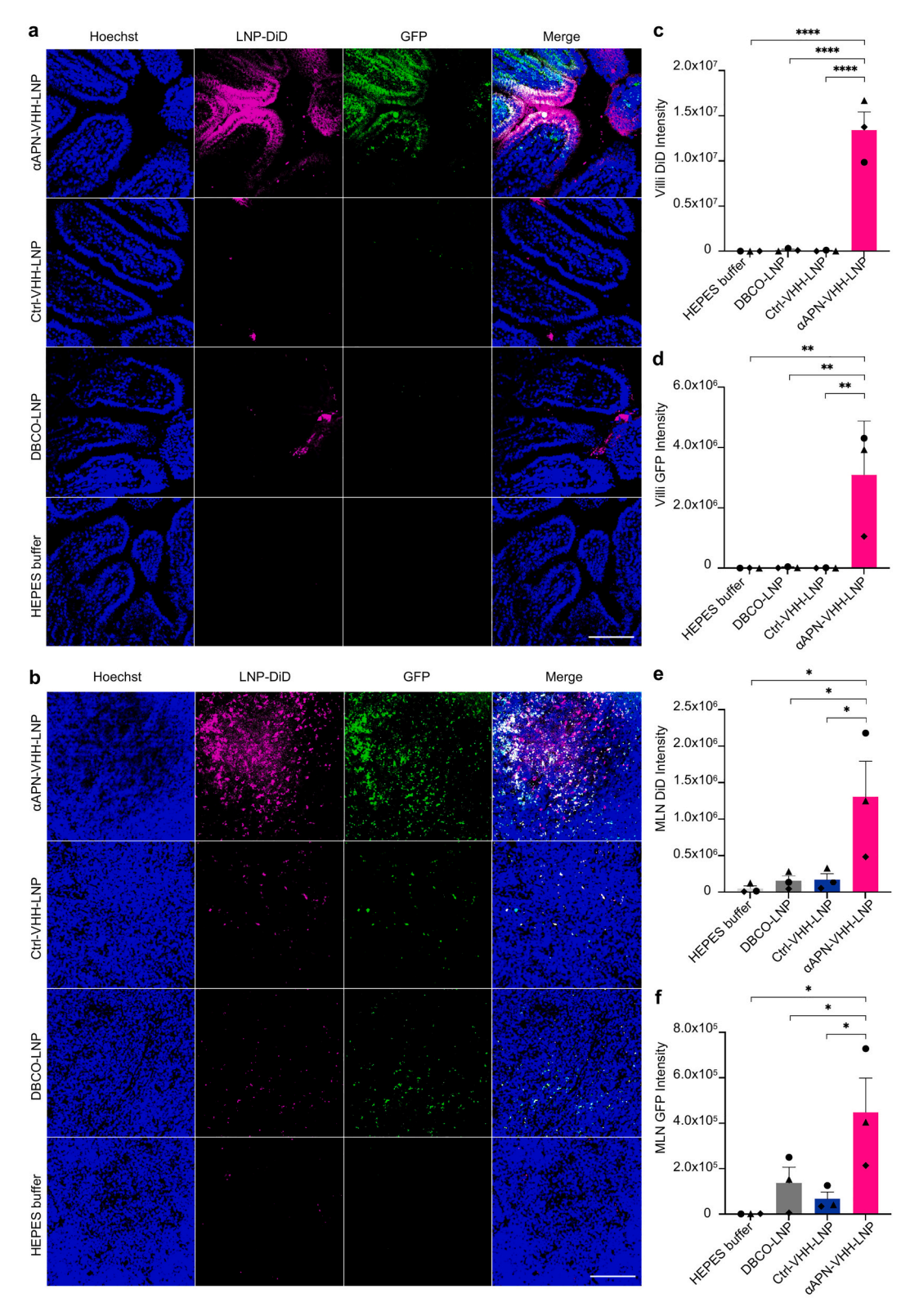


**Fig. 6.** αAPN-VHH-LNPs mediate targeted delivery of mRNA to the small intestinal epithelium and mesenteric lymph nodes (MLNs) in vivo. a,b)Representative confocal images of jejunal villi a) and MLNs b) collected 6 h after luminal administration of DiD-labeled mRNA-LNPs. Tissue sections were fixed with 4 % PFA, nuclei were stained with Hoechst (blue), VHH-LNPs were labeled with DiD (magenta), and GFP expression is shown in green. Colocalization of DiD and GFP signals appears white in the merged images. Images are representative of 3 piglets. Scale bar: 200 μm. c−f) Quantification of DiD c, e) and GFP d, f) fluorescence intensity in villi c,d) and MLNs e,f). Each point represents the average of 4 field views from 2 sections per condition, with n = 3 pigs( Pig 1, Pig 2, Pig 3). Data analyzed by one-way ANOVA. \*P < 0.05, \*P < 0.01, \*\*\*\*P < 0.001.

across the gut epithelium [56-59].

Using apical-out intestinal enteroids and fluorescence lifetime imaging microscopy (FLIM), we demonstrated that APN-targeted mRNA-LNPs are transported across the epithelial barrier in a physiologically relevant 3D model. In these polarized epithelial cells, GFP expression following LNP uptake also indicated cytoplasmic delivery of mRNA. However, we speculate that in cases of pathway saturation, a fraction of the vesicles may be diverted from the transcytosis pathway and guided toward endosomal escape and mRNA translation. A similar observation was made in the gut ligated loop experiment in piglets. We observed uptake of GFP-loaded  $\alpha$ APN-VHH-LNPs by intestinal epithelial cells in the jejunal villi, which was absent in the control groups. This uptake resulted in delivery of mRNA to and subsequent GFP expression by gut epithelial cells. Importantly, APN-targeted mRNA-LNPs were also transported through the gut epithelial cells and released at the basolateral surface, where they were taken up by subepithelial cells, most likely antigen-presenting cells. The presence of DiD and GFP in mesenteric lymph nodes draining the gut tissues stimulated with APN-targeted mRNA-LNPs suggests that at least a part of these molecules were delivered by antigen-presenting cells that migrated from the subepithelial compartment to the lymph nodes. Given that APN is also expressed on certain APCs and immune cells, such as monocytes, macrophages, and specific dendritic cell subsets (e.g., cDC1) [60], future studies are warranted to investigate whether these APN-expressing immune cells preferentially take up αAPN-VHH-LNPs. This targeted uptake by specific immune subsets, particularly cDC1, could open opportunities to tailor and enhance the resulting immune response. Besides, a low GFP expression and DiD signal were also observed in lymph nodes draining tissues with control LNPs. Although no significant LNP accumulation or mRNA translation was observed in the villi of these groups, some LNP uptake and GFP expression was evident in the crypt regions. This suggests that in the absence of targeted APN-mediated uptake a small fraction of LNPs may still be internalized by crypt-residing cells [61]. Of note, mRNA delivery and translation seemed to be more efficient in vivo than in vitro. This might be attributed to higher LNP concentration administered to the intestinal lumen, which likely enhanced uptake. However, only APN-targeted LNPs achieved substantial tissue delivery and mRNA translation, underscoring the importance of receptormediated targeting. Together, these results align with our in vitro findings and our previous findings showing that APN-targeted antibodyantigen fusion constructs are transported across the small intestinal epithelium and, upon their release, are taken up by gut resident antigenpresenting cells, which then migrate to the local draining lymph node to initiate immune responses [31]. Further in vivo studies should assess the prophylactic and therapeutic potential of our delivery system.

Despite demonstrating enhanced targeting ability and effective mRNA delivery both *in vitro* and *in vivo*, the current αAPN-VHH-LNP platform requires further optimization. A major challenge is their stability in the gut environment, where acidic pH and enzymes can degrade LNPs [62]. One strategy to overcome gastric degradation is neutralizing the stomach pH using proton pump inhibitors or bicarbonate buffer to allow LNPs to pass intact to the small intestine [30]. Notably, bicarbonate buffer is used with the licensed oral cholera vaccine Dukoral® [63]. However, LNP stability in such neutralizing solutions needs to be confirmed. Another strategy is to lyophilize the LNPs and formulate them in enteric-coated capsules [64]. This would allow releasing the LNPs directly in the small intestine and potentially achieve long-term stability. Further experiments are needed to verify the LNP stability and function after the freeze-drying process.

Furthermore, we recognize that optimizing the ionizable lipid component could potentially enhance mRNA delivery efficiency. A recent study comparing ionizable lipids found that LNPs formulated with SM-102 achieved higher *in vitro* transfection potency than those using ALC-0315, MC3, or DOTAP [65]. Additionally, SM-102-based LNPs demonstrated superior *in vivo* protein expression and pharmacokinetic performance, including approximately three times greater

plasma bioavailability than ALC-0315 in mouse models [66]. Based on these findings, our next step will be to synthesize SM-102–based  $\alpha APN-VHH-LNPs$  and benchmark their performance in gut delivery, with the goal of enhanced stability and mRNA delivery efficiency. In addition, the mRNA species might be changed to increase the therapeutic dose delivered to the gut tissues. Our mRNA construct was engineered with a poly(A) tail and a Cap1 structure, enhancing stability and translation efficiency, with chemical modifications such as 5-methylcytidine for increased stability and reduced immune activation. Future work could explore whether loading self-amplifying RNA in the LNPs can improve protein expression levels in the gut tissues [67,68].

Noteworthy, APN is also abundantly expressed by various tumors, making it an attractive target for cancer immunotherapy [69]. Studies suggest that targeting APN could enhance nanoparticle-mediated precision delivery of therapeutics to tumor cells, reducing off-target effects and increasing therapeutic efficacy [70]. Adapting our platform for cancer treatment holds promise for improving therapeutic outcomes in cancer immunotherapy and reducing adverse effects by focusing delivery to tumors.

#### 5. Conclusions

Here, we developed an APN-targeted mRNA-LNP delivery system using APN-specific VHHs to enable cell-specific mRNA delivery. Through a two-step click chemistry approach, we functionalized the mRNA-LNPs with VHHs, resulting in cellular uptake and transport across the small intestinal epithelium. This mRNA-delivery platform has potential applications in oral vaccination and immunotherapy, and potentially in cancer therapy. Further adjustments to the lipid composition and mRNA species could enhance its versatility and effectiveness. In summary, this targeted mRNA-LNP system offers a promising tool for cell-specific delivery of mRNA therapeutics to advance developments in oral vaccination, gene editing, protein replacement therapy, and immunotherapy.

# CRediT authorship contribution statement

Linglong Chen: Writing – review & editing, Writing – original draft, Visualization, Validation, Software, Methodology, Investigation, Formal analysis, Data curation, Conceptualization. Hans Van Der Weken: Writing – review & editing, Supervision, Funding acquisition, Conceptualization. Olivier Zwaenepoel: Writing – review & editing, Validation, Supervision, Methodology. Irina A. Okkelman: Writing – review & editing, Supervision, Methodology. Justine Aelvoet: Supervision, Resources, Methodology. Emma Van Denberghe: Project administration, Methodology. Jan Gettemans: Resources, Methodology. Ruslan I. Dmitriev: Supervision, Methodology. Bruno G. De Geest: Resources, Methodology. Eric Cox: Project administration, Funding acquisition, Conceptualization. Bert Devriendt: Writing – review & editing, Validation, Supervision, Project administration, Funding acquisition, Conceptualization.

# **Ethical statement**

This experiment was reviewed and approved by the Ethical Committee of the Faculties of Veterinary Medicine and Bioscience Engineering at Ghent University, following the Belgian law on animal experimentation (EC2024/038).

# Declaration of generative AI and AI-assisted technologies in the writing process

During the preparation of this work, the author used ChatGPT in order to improve language and readability. After using this tool/service, the author reviewed and edited the content as needed and took full responsibility for the content of the publication.

#### **Funding**

L.C. is supported by a scholarship from the China Scholarship Council (CSC). This work was supported by grants from the Special Research Fund of Ghent University (BOF/STA/202009/021; BOF/BAS/2015/0029/01), the industrial research fund of Ghent University (F2023/IOF-Equip/099), and the Research Foundation Flanders (FWO-Vlaanderen; G065723N). We acknowledge the CORE facility flow cytometry for the use of their equipment (BOF/COR/2022/001).

### Declaration of competing interest

We declare that we have no financial and personal relationships with other people or organizations that can inappropriately influence our work, and there is no conflict of interest regarding the publication of this paper.

# Acknowledgments

The authors sincerely thank Dr. Matthias Dierick for his expert guidance during the dosing experiments and for his support with enteroid maintenance and splitting. We are also grateful to Hang Zhou for his assistance with enteroid culture and FLIM imaging, and to Emma Vanbeylen for her help during the in vivo experiments and anesthesia procedures. We thank Nidhal Guendouz for her support in tissue collection.

### Appendix A. Supplementary data

Supplementary data to this article can be found online at https://doi.org/10.1016/j.jconrel.2025.114365.

# Data availability

Data will be made available on request.

## References

- X. Hou, T. Zaks, R. Langer, Y. Dong, Lipid nanoparticles for mRNA delivery, Nat. Rev. Mater. 6 (2021) 1078–1094.
- [2] N. Pardi, M.J. Hogan, F.W. Porter, D. Weissman, mRNA vaccines—a new era in vaccinology, Nat. Rev. Drug Discov. 17 (2018) 261–279.
- [3] S. Kwon, M. Kwon, S. Im, K. Lee, H. Lee, mRNA vaccines: the most recent clinical applications of synthetic mRNA, Arch. Pharm. Res. 45 (2022) 245–262.
- [4] K.A. Hajj, K.A. Whitehead, Tools for translation: non-viral materials for therapeutic mRNA delivery, Nat. Rev. Mater. 2 (2017) 1–17.
- [5] L.M. Kranz, M. Diken, H. Haas, S. Kreiter, C. Loquai, K.C. Reuter, M. Meng, D. Fritz, F. Vascotto, H. Hefesha, Systemic RNA delivery to dendritic cells exploits antiviral defence for cancer immunotherapy, Nature 534 (2016) 396–401.
- [6] C. Meng, Z. Chen, G. Li, T. Welte, H. Shen, Nanoplatforms for mRNA therapeutics, Adv. Ther. 4 (2021) 2000099.
- [7] W. Zhao, X. Hou, O.G. Vick, Y. Dong, RNA delivery biomaterials for the treatment of genetic and rare diseases, Biomaterials 217 (2019) 119291.
- [8] N. Pardi, M.J. Hogan, D. Weissman, Recent advances in mRNA vaccine technology, Curr. Opin. Immunol. 65 (2020) 14–20.
- [9] P.S. Kowalski, A. Rudra, L. Miao, D.G. Anderson, Delivering the messenger: advances in technologies for therapeutic mRNA delivery, Mol. Ther. 27 (2019) 710, 728
- [10] S.P. Teo, Review of COVID-19 mRNA vaccines: BNT162b2 and mRNA-1273, J. Pharm. Pract. 35 (2022) 947–951.
- [11] L. Schoenmaker, D. Witzigmann, J.A. Kulkarni, R. Verbeke, G. Kersten, W. Jiskoot, D.J. Crommelin, mRNA-lipid nanoparticle COVID-19 vaccines: structure and stability, Int. J. Pharm. 601 (2021) 120586.
- [12] G.T. Kozma, T. Mészáros, P. Berényi, R. Facskó, Z. Patkó, C.Z. Oláh, A. Nagy, T. G. Fülöp, K.A. Glatter, T. Radovits, Role of anti-polyethylene glycol (PEG) antibodies in the allergic reactions to PEG-containing Covid-19 vaccines: evidence for immunogenicity of PEG, Vaccine 41 (2023) 4561–4570.
- [13] T. Boettler, B. Csernalabics, H. Salié, H. Luxenburger, L. Wischer, E.S. Alizei, K. Zoldan, L. Krimmel, P. Bronsert, M. Schwabenland, SARS-CoV-2 vaccination can elicit a CD8 T-cell dominant hepatitis, J. Hepatol. 77 (2022) 653–659.
- [14] E.J. Anderson, N.G. Rouphael, A.T. Widge, L.A. Jackson, P.C. Roberts, M. Makhene, J.D. Chappell, M.R. Denison, L.J. Stevens, A.J. Pruijssers, Safety and immunogenicity of SARS-CoV-2 mRNA-1273 vaccine in older adults, N. Engl. J. Med. 383 (2020) 2427–2438.

- [15] E. Kon, N. Ad-El, I. Hazan-Halevy, L. Stotsky-Oterin, D. Peer, Targeting cancer with mRNA-lipid nanoparticles: key considerations and future prospects, Nat. Rev. Clin. Oncol. 20 (2023) 739–754.
- [16] M. Qiu, Y. Tang, J. Chen, R. Muriph, Z. Ye, C. Huang, J. Evans, E.P. Henske, Q. Xu, Lung-selective mRNA delivery of synthetic lipid nanoparticles for the treatment of pulmonary lymphangioleiomyomatosis, Proc. Natl. Acad. Sci. 119 (2022) e2116271119.
- [17] Z. Yang, Y. Liu, K. Zhao, W. Jing, L. Gao, X. Dong, Y. Wang, M. Han, C. Shi, C. Tang, Dual mRNA co-delivery for in situ generation of phagocytosis-enhanced CAR macrophages augments hepatocellular carcinoma immunotherapy, J. Ophthalmol. Clinics Res. 360 (2023) 718–733.
- [18] J. Chen, Z. Ye, C. Huang, M. Qiu, D. Song, Y. Li, Q. Xu, Lipid nanoparticle-mediated lymph node-targeting delivery of mRNA cancer vaccine elicits robust CD8+ T cell response, Proc. Natl. Acad. Sci. 119 (2022) e2207841119.
- [19] J. Li, H. Wang, Selective organ targeting nanoparticles: from design to clinical translation, Nanoscale Horiz. 8 (2023) 1155–1173.
- [20] Q. Cheng, T. Wei, L. Farbiak, L.T. Johnson, S.A. Dilliard, D.J. Siegwart, Selective organ targeting (SORT) nanoparticles for tissue-specific mRNA delivery and CRISPR—Cas gene editing, Nat. Nanotechnol. 15 (2020) 313–320.
- [21] X. Wang, S. Liu, Y. Sun, X. Yu, S.M. Lee, Q. Cheng, T. Wei, J. Gong, J. Robinson, D. Zhang, Preparation of selective organ-targeting (SORT) lipid nanoparticles (LNPs) using multiple technical methods for tissue-specific mRNA delivery, Nat. Protoc. 18 (2023) 265–291.
- [22] A. Solorio-Rodríguez, V. Escamilla-Rivera, M. Uribe-Ramírez, A. Chagolla, R. Winkler, C. García-Cuellar, A. De Vizcaya-Ruiz, A comparison of the human and mouse protein corona profiles of functionalized SiO 2 nanocarriers, Nanoscale 9 (2017) 13651–13660.
- [23] H.C. Geisler, A.A. Ghalsasi, H.C. Safford, K.L. Swingle, A.S. Thatte, A.J. Mukalel, N. Gong, A.G. Hamilton, E.L. Han, B.E. Nachod, EGFR-targeted ionizable lipid nanoparticles enhance in vivo mRNA delivery to the placenta, J. Control. Release 371 (2024) 455–469.
- [24] R. Liu, R.J. Oldham, E. Teal, S.A. Beers, M.S. Cragg, Fc-engineering for modulated effector functions—improving antibodies for cancer treatment, Antibodies 9 (2020) 64.
- [25] S. Muyldermans, Nanobodies: natural single-domain antibodies, Annu. Rev. Biochem. 82 (2013) 775–797.
- [26] Y. Ren, W. Wu, X. Zhang, The feasibility of oral targeted drug delivery: gut immune to particulates? Acta Pharm. Sin. B 13 (2023) 2544–2558.
- [27] J.L. Bird, R. Simpson, D. Vllasaliu, A.D. Goddard, Neurotensin receptor 1 facilitates intracellular and transepithelial delivery of macromolecules, Eur. J. Pharm. Biopharm. 119 (2017) 300–309.
- [28] M. Yoshida, K. Kobayashi, T.T. Kuo, L. Bry, J.N. Glickman, S.M. Claypool, A. Kaser, T. Nagaishi, D.E. Higgins, E. Mizoguchi, Neonatal Fc receptor for IgG regulates mucosal immune responses to luminal bacteria, J. Clin. Invest. 116 (2006) 2142–2151.
- [29] S. Pinto, M. Hosseini, S.T. Buckley, W. Yin, J. Garousi, T. Gräslund, S. van Ijzendoorn, H.A. Santos, B. Sarmento, Nanoparticles targeting the intestinal fc receptor enhance intestinal cellular trafficking of semaglutide, J. Control. Release 366 (2024) 621–636.
- [30] H. Van der Weken, H.R. Jahantigh, E. Cox, B. Devriendt, Targeted delivery of oral vaccine antigens to aminopeptidase N protects pigs against pathogenic E. Coli challenge infection, Front. Immunol. 14 (2023) 1192715.
- [31] H. Van der Weken, R. Sanz Garcia, N.N. Sanders, E. Cox, B. Devriendt, Antibody-mediated targeting of antigens to intestinal aminopeptidase n elicits gut IgA responses in pigs, Front. Immunol. 12 (2021) 753371.
- [32] K. Baert, B.G. De Geest, R. De Rycke, A.B. da Fonseca Antunes, H. De Greve, E. Cox, B., Devriendt, β-glucan microparticles targeted to epithelial APN as oral antigen delivery system, J. Control. Release 220 (2015) 149–159.
- [33] S. Bakshi, R.S. Garcia, H. Van der Weken, A. Tharad, S. Pandey, P. Juarez, V. Virdi, B. Devriendt, E. Cox, A. Depicker, Evaluating single-domain antibodies as carriers for targeted vaccine delivery to the small intestinal epithelium, J. Control. Release 321 (2020) 416–429.
- [34] T. Hebbrecht, J. Liu, O. Zwaenepoel, G. Boddin, C. Van Leene, K. Decoene, A. Madder, K. Braeckmans, J. Gettemans, Nanobody click chemistry for convenient site-specific fluorescent labelling, single step immunocytochemistry and delivery into living cells by photoporation and live cell imaging, New Biotechnol. 59 (2020) 33-43.
- [35] B. Vermeire, L.M. Gonzalez, R.J. Jansens, E. Cox, B. Devriendt, Porcine small intestinal organoids as a model to explore ETEC-host interactions in the gut, Vet. Res. 52 (2021) 94.
- [36] S.-S. Joo, B.-H. Gu, Y.-J. Park, C.-Y. Rim, M.-J. Kim, S.-H. Kim, J.-H. Cho, H.-B. Kim, M. Kim, Porcine intestinal apical-out organoid model for gut function study, Animals 12 (2022) 372.
- [37] A.C. Debruyne, I.A. Okkelman, N. Heymans, C. Pinheiro, A. Hendrix, M. Nobis, S. M. Borisov, R.I. Dmitriev, Live microscopy of multicellular spheroids with the multimodal near-infrared nanoparticles reveals differences in oxygenation gradients, ACS Nano 18 (2024) 12168–12186.
- [38] F. Njeru, O. Zwaenepoel, G. Haesaert, G. Misinzo, K. De Jonghe, J. Gettemans, Development of nanobodies against the coat protein of maize chlorotic mottle virus, FEBS Open Bio 14 (2024) 1746–1757.
- [39] M. Ishii, Y. Fukuoka, S. Deguchi, H. Otake, T. Tanino, N. Nagai, Energy-dependent endocytosis is involved in the absorption of indomethacin nanoparticles in the small intestine, Int. J. Mol. Sci. 20 (2019) 476.
- [40] Y.-B. Yin, S.-G. Guo, D. Wan, X. Wu, Y.-L. Yin, Enteroids: promising in vitro models for studies of intestinal physiology and nutrition in farm animals, J. Agric. Food Chem. 67 (2019) 2421–2428.

- [41] R.I. Dmitriev, X. Intes, M.M. Barroso, Luminescence lifetime imaging of threedimensional biological objects, J. Cell Sci. 134 (2021) 1–17.
- [42] P. Eiring, R. McLaughlin, S.S. Matikonda, Z. Han, L. Grabenhorst, D.A. Helmerich, M. Meub, G. Beliu, M. Luciano, V. Bandi, Targetable Conformationally restricted Cyanines enable photon-count-limited applications, Angew. Chem. Int. Ed. 60 (2021) 26685–26693.
- [43] M. Huang, X. Liang, Z. Zhang, J. Wang, Y. Fei, J. Ma, S. Qu, L. Mi, Carbon dots for intracellular pH sensing with fluorescence lifetime imaging microscopy, Nanomaterials 10 (2020) 604.
- [44] J. Simon, M. Fichter, G. Kuhn, M. Brückner, C. Kappel, J. Schunke, T. Klaus, S. Grabbe, K. Landfester, V. Mailänder, Achieving dendritic cell subset-specific targeting in vivo by site-directed conjugation of targeting antibodies to nanocarriers, Nano Today 43 (2022) 101375.
- [45] P. Bannas, J. Hambach, F. Koch-Nolte, Nanobodies and nanobody-based human heavy chain antibodies as antitumor therapeutics, Front. Immunol. 8 (2017) 309808.
- [46] S.E. Gratton, P.A. Ropp, P.D. Pohlhaus, J.C. Luft, V.J. Madden, M.E. Napier, J. M. DeSimone, The effect of particle design on cellular internalization pathways, Proc. Natl. Acad. Sci. 105 (2008) 11613–11618.
- [47] T.-G. Iversen, T. Skotland, K. Sandvig, Endocytosis and intracellular transport of nanoparticles: present knowledge and need for future studies, Nano Today 6 (2011) 176-185
- [48] G. Sahay, D.Y. Alakhova, A.V. Kabanov, Endocytosis of nanomedicines, J. Control. Release 145 (2010) 182–195.
- [49] Y. Xie, J. Rufo, R. Zhong, J. Rich, P. Li, K.W. Leong, T.J. Huang, Microfluidic isolation and enrichment of nanoparticles, ACS Nano 14 (2020) 16220–16240.
- [50] I. Van Zundert, M. Bravo, O. Deschaume, P. Cybulski, C. Bartic, J. Hofkens, H. Uji-i, B. Fortuni, S. Rocha, Versatile and robust method for antibody conjugation to nanoparticles with high targeting efficiency, Pharmaceutics 13 (2021) 2153.
- [51] G. Zhao, L. Xue, H.C. Geisler, J. Xu, X. Li, M.J. Mitchell, A.E. Vaughan, Precision treatment of viral pneumonia through macrophage-targeted lipid nanoparticle delivery, Proc. Natl. Acad. Sci. 121 (2024) e2314747121.
- [52] E. Chabrol, J. Stojko, A. Nicolas, T. Botzanowski, B. Fould, M. Antoine, S. Cianférani, G. Ferry, J.A. Boutin, VHH characterization. Recombinant VHHs: Production, characterization and affinity, Anal. Biochem. 589 (2020) 113491.
- [53] L.E. Swart, C.A. Koekman, C.W. Seinen, H. Issa, M. Rasouli, R.M. Schiffelers, O. Heidenreich, A robust post-insertion method for the preparation of targeted siRNA LNPs, Int. J. Pharm. 620 (2022) 121741.
- [54] M.H. Zaleski, L.S. Chase, E.D. Hood, Z. Wang, J. Nong, C.L. Espy, M.E. Zamora, J. Wu, L.J. Morrell, V.R. Muzykantov, Conjugation chemistry markedly impacts toxicity and biodistribution of targeted nanoparticles, mediated by complement activation, Adv. Mater. 37 (2025) 2409945.
- [55] J.L. Seitchik, J.C. Peeler, M.T. Taylor, M.L. Blackman, T.W. Rhoads, R.B. Cooley, C. Refakis, J.M. Fox, R.A. Mehl, Genetically encoded tetrazine amino acid directs rapid site-specific in vivo bioorthogonal ligation with trans-cyclooctenes, J. Am. Chem. Soc. 134 (2012) 2898–2901.

- [56] O.A. Weisz, H. Fölsch, Molecular Mechanisms of Apical and Basolateral Sorting in Polarized Epithelial Cells, Ion Channels and Transporters of Epithelia in Health and Disease, 2016, pp. 279–302.
- [57] P.L. Tuma, A.L. Hubbard, Transcytosis: crossing cellular barriers, Physiol. Rev. 83 (2003) 871–932.
- [58] Y.T. Ho, R.D. Kamm, J.C.Y. Kah, Influence of protein corona and caveolaemediated endocytosis on nanoparticle uptake and transcytosis, Nanoscale 10 (2018) 12386–12397.
- [59] H. Fölsch, Regulation of membrane trafficking in polarized epithelial cells, Curr. Opin. Cell Biol. 20 (2008) 208–213.
- [60] G. Auray, S.C. Talker, I. Keller, S. Python, M. Gerber, M. Liniger, L. Ganges, R. Bruggmann, N. Ruggli, A. Summerfield, High-resolution profiling of innate immune responses by porcine dendritic cell subsets in vitro and in vivo, Front. Immunol. 11 (2020) 1429.
- [61] Y. Qin, Z. Wang, H. Chen, G. Nie, R. Zhao, Oral nanoparticle therapy for inflammatory bowel disease by Paneth cell regulation and mucus layer remodeling, Matter 8 (2025).
- [62] A. Zafar, R. Arshad, A. Ur, N. Rehman, H. Akhtar Ahmed, Recent developments in oral delivery of vaccines using nanocarriers, Vaccines 11 (2023) 490.
- [63] T. Jelinek, H. Kollaritsch, Vaccination with Dukoral® against travelers' diarrhea (ETEC) and cholera, Expert Rev. Vaccines 7 (2008) 561–567.
- [64] Y. Fan, D. Rigas, L.J. Kim, F.-P. Chang, N. Zang, K. McKee, C.C. Kemball, Z. Yu, P. Winkler, W.-C. Su, Physicochemical and structural insights into lyophilized mRNA-LNP from lyoprotectant and buffer screenings, J. Control. Release 373 (2024) 727–737.
- [65] B. Binici, Z. Rattray, A. Zinger, Y. Perrie, Exploring the impact of commonly used ionizable and pegylated lipids on mRNA-LNPs: a combined in vitro and preclinical perspective, J. Control. Release 377 (2025) 162–173.
- [66] Y. Ren, L. Lin, M. Abdallah, X. Zhu, H. Liu, S.A. Fabb, T.J. Payne, C.W. Pouton, A. P. Johnston, N.L. Trevaskis, Impact of ionizable lipid type on the pharmacokinetics and biodistribution of mRNA-lipid nanoparticles after intravenous and subcutaneous injection, J. Control. Release 113945 (2025).
- [67] E. De Lombaerde, X. Cui, Y. Chen, Z. Zhong, J. Deckers, G. Mencarelli, L. Opsomer, H. Wang, J. De Baere, S. Lienenklaus, Amplification of protein expression by self-amplifying mRNA delivered in lipid nanoparticles containing a β-Aminoester Ionizable lipid correlates with reduced innate immune activation, ACS Nano 18 (2024) 28311–28324.
- [68] A.-K. Minnaert, H. Vanluchene, R. Verbeke, I. Lentacker, S.C. De Smedt, K. Raemdonck, N.N. Sanders, K. Remaut, Strategies for controlling the innate immune activity of conventional and self-amplifying mRNA therapeutics: getting the message across, Adv. Drug Deliv. Rev. 176 (2021) 113900.
- [69] S. Nohara, K. Kato, D. Fujiwara, N. Sakuragi, K. Yanagihara, Y. Iwanuma, Y. Kajiyama, Aminopeptidase N (APN/CD13) as a target molecule for scirrhous gastric cancer, Clin. Res. Hepatol. Gastroenterol. 40 (2016) 494–503.
- [70] E. Grieger, G. Gresch, J. Niesen, M. Woitok, S. Barth, R. Fischer, R. Fendel, C. Stein, Efficient targeting of CD13 on cancer cells by the immunotoxin scFv13–ETA' and the bispecific scFv [13xds16], J. Cancer Res. Clin. Oncol. 143 (2017) 2159–2170.